PNL-10815
UC-2030

# Dilution Physics Modeling Dissolution/Precipitation Chemistry

Y. Onishi
H. C. Reid
D. S. Trent

September 1995

Prepared for
the U.S. Department of Energy
Under Contract DE-AC06-76RLO 1830

Pacific Northwest Laboratory
Richland, Washington 99352

# Executive Summary

This report documents progress made to date on integrating dilution/precipitation chemistry and new physical models into the TEMPEST thermal-hydraulics computer code. Implementation of dissolution/precipitation chemistry models is necessary for predicting nonhomogeneous, time-dependent, physical/chemical behavior of tank wastes with and without a variety of possible engineered remediation and mitigation activities. Such behavior includes chemical reactions, gas retention, solids resuspension, solids dissolution and generation, solids settling/rising, and convective motion of physical and chemical species. Thus this model development is important from the standpoint of predicting the consequences of various engineered activities, such as mitigation by dilution, retrieval, or pretreatment, that can affect safe operations.

The integration of a dissolution/precipitation chemistry module allows the various phase species concentrations to enter into the physical calculations that affect the TEMPEST hydrodynamic flow calculations. The yield strength model of non-Newtonian sludge correlates yield to a power function of solids concentration. Likewise, shear stress is concentration-dependent, and the dissolution/precipitation chemistry calculations develop the species concentration evolution that produces fluid flow resistance changes. Dilution of waste with pure water, molar concentrations of sodium hydroxide, and other chemical streams can be analyzed for the reactive species changes and hydrodynamic flow characteristics.

Preliminary model testing confirmed the feasibility of incorporating a chemical model into TEMPEST to predict precipitation/dissolution effects on tank waste transport modeling; however, it also indicated that wider and more flexible selections of reacting chemical species and other variables (including pH) were needed to handle complex tank waste compositions affecting physical properties and rheology. This preliminary testing led to an approach for modeling the interactions of aqueous chemical reactions, dissolution/precipitation, adsorption/desorption (when applicable), and possibly gaseous reactions. To account for these synergistic effects, the equilibrium chemical code, GMIN, and associated chemical kinetics models were implemented into the TEMPEST thermal-hydraulics code.

The modified TEMPEST code was tested for simplified situations that involved the decay of jet-induced motion and dilution injection to test the model's computational behavior. Although simplified, these test cases resemble actual physical and chemical processes applicable to the Hanford waste tanks. These modeling exercises revealed that solids dissolution and precipitation are important processes that should be incorporated into tank waste dilution evaluations.

When TEMPEST is fully integrated with chemical reactions and other physical modeling improvements, it will be able to more broadly and reliably address complex interacting chemical and physical processes that are naturally occurring, as well as those that are associated with tank operational activities, including dilution of tank wastes, mixing of various tank wastes, gas retention, and waste pretreatment processes.

# Acknowledgments

This work was supported jointly by the Tank Waste Safety Programs Hydrogen Mitigation and Flammable Gas. The amount of progress made on this very difficult task could not have been achieved without this joint support.

Additionally, the reported progress would have been impossible (within the time and funding constraints) without the vast amount of information and guidance gained from the Pretreatment program. In this regard, the authors wish to extend their appreciation to Drs. A. R. Felmy and J. R. Rustad for their valuable guidance and assistance in incorporating equilibrium and kinetic chemical reaction modeling capabilities into the TEMPEST code. Dr. Felmy's GMIN computer code proved invaluable to us in this effort.

# Contents


Executive Summary . . . . . iii

Acknowledgments . . . . . v

1.0 Introduction . . . . . 1.1

1.1 Hydrodynamics and Transport: Constituents and Chemical Species . . . . . 1.2

1.2 Chemical Constituent Species Transport . . . . . 1.4

2.0 Technical Approach . . . . . 2.1

2.1 Dissolution And Precipitation Chemistry . . . . . 2.1

2.1.1 Objective of Dissolution/Precipitation Modeling . . . . . 2.1

2.1.2 Basic Technical Approach . . . . . 2.2

2.1.3 Specific Technical Approach . . . . . 2.3

2.1.4 Data Requirements for Dissolution/Precipitation Modeling . . . . . 2.6

2.2 Physical Property and Rheological Modeling . . . . . 2.6

3.0 Model Applications . . . . . 3.1

3.1 Test Conditions and Modeling Results Summary . . . . . 3.1

3.1.1 Decayed Jet Tank Segment Model Set . . . . . 3.2

3.1.2 Dilution Injection Model . . . . . 3.5

3.2 Detailed Decayed Jet Tank Segment Model Results and Evaluations . . . . . 3.8

3.2.1 Results of the Decayed Jet Tank Segment Model Runs . . . . . 3.9

3.2.2 Evaluations of the Decayed Jet Tank Segment Model Runs . . . . . 3.10

3.3 Detailed Dilution Injection Model Results and Evaluations . . . . . 3.13

3.3.1 Results of the Dilution Injection Model Runs . . . . . 3.13

3.3.2 Evaluations of the Dilution Injection Model Runs . . . . . 3.14

4.0 Conclusions and Recommendations . . . . . 4.1

5.0 References . . . . . 5.1

# Figures


3.1 Decayed Jet Tank Segment Model . . . . . 3.2

3.2 Waste Tank Dilution Injection Model . . . . . 3.6

3.3 Dilution Injection Model Region . . . . . 3.7

3.4 $NaNO_3$(s) at 0.4 Second for Case 5 . . . . . 3.17

3.5 $NaNO_3$(s) and $NaNO_2$(s) for Case 1 . . . . . 3.18

3.6 Nonreactive Solids 3 and 4, $H_2/N_2$ Gas at Location 1 for Case 1 . . . . . 3.18

3.7 $NaNO_3$(s) Over 10 Seconds at Location 1 for Case 1 . . . . . 3.19

3.8 $NaNO_3$(s) at One Minute for Case 1 . . . . . 3.19

3.9 $NaNO_3$(s) at 15 Minutes for Case 1 . . . . . 3.20

3.10 $NaNO_2$(s) at 15 Minutes for Case 1 . . . . . 3.20

3.11 Velocity Distribution at 15 Minutes for Case 1 . . . . . 3.21

3.12 $NaNO_3$(s) Over 15 Minutes at Location 1 for Case 2 . . . . . 3.21

3.13 $NaNO_3$(s) at One Minute for Case 2 . . . . . 3.22

3.14 $NaNO_3$(s) at 15 Minutes for Case 2 . . . . . 3.22

3.15 Velocity Distribution at 15 Minutes for Case 2 . . . . . 3.23

3.16 $NaNO_3$(s) Over 15 Minutes at Location 1 for Cases 1–3 . . . . . 3.23

3.17 $NaNO_3$(s) at One Minute for Case 3 . . . . . 3.24

3.18 $NaNO_3$(s) at 15 Minutes for Case 3 . . . . . 3.24

3.19 Velocity Distribution at 15 Minutes for Case 3 . . . . . 3.25

3.20 $NaNO_3$(s) Over One Minute at Location 1 for Case 4 . . . . . 3.25

3.21 $NaNO_3$(s) at 30 Seconds for Case 4 . . . . . 3.26

3.22 $NaNO_3$(s) at One Minute for Case 4 . . . . . 3.26

3.23 $NaNO_3$(s) at 30 Seconds for Case 5 . . . . . 3.27

3.24 Velocity Distribution at 0.476 Second for Case 4 . . . . . 3.27

3.25 $NaNO_3$(s) and $NaNO_2$(s) over 15 Minutes for Case 1 . . . . . 3.28

3.26 Nonreactive Solid 4 and $H_2/N_2$ Gas over 15 Minutes at Location 1 for Case 1 . . . . 3.28

3.27 $NaNO_3$(s) at 15 Minutes for Case 1 . . . . . 3.29

3.28 Velocity Distribution at 15 Minutes for Case 1 . . . . . 3.29

3.29 $NaNO_3$(s) Over 15 Minutes at Location 1 for Cases 1–3 . . . . . 3.30

3.30 $NaNO_3$(s) Over 15 Minutes for Case 3 . . . . . 3.30

3.31 $NaNO_3$(s) Over One Minute at Location 1 for Case 4 . . . . . 3.31

3.32 $NaNO_3$(s) at 100 Seconds for Case 4 . . . . . 3.31

3.33 $NaNO_3$(s) at 100 Seconds for Case 5 . . . . . 3.32

## Tables

3.1 Initial Concentrations for Decayed Jet Tank Segment and Dilution Injection Models . . . 3.3

3.2 Predicted Chemical Concentrations (kg/m³) at 15 Minutes for Cases 1, 2, and 3 and at 30 Seconds for Case 4 of the Decayed Jet Tank Segment Model . . . . . 3.12

3.3 Predicted Chemical Concentrations (kg/m³) at 15 Minutes for Cases 1 through 3 of the Dilution Injection Model . . . . . 3.15

# 1.0 Introduction

Waste in Tank 241-SY-101 on the Hanford Site in Washington State generates hydrogen, nitrous oxide, and nitrogen gases. Existing tank data are consistent with the interpretation that gases are uniformly generated in the tank. Pederson and Strachan (1993) summarized the importance of solids on gas release this way: "Solid settling rates and slurry rheological properties are consistent with the hypothesis that the fracture of dendritic sodium nitrite grains is the controlling factor of in determining when gas is released."

Installation of a mixer pump in 1993 has effectively mitigated the problem of large episodic gas releases in the tank. However, mitigation by mixing has occurred at significant expense, including the operational expenses associated with continued pump operations. These costs are required to maintain the tank in a mitigated state while the waste awaits eventual retrieval and transport to a processing facility.

Dilution has been proposed as an alternative long-term waste tank mitigation strategy because of its potential to provide mitigation in the absence of routine pump mixing (Babad et al. 1992; Stewart et al. 1994). Dilution is proposed to mitigate the episodic gas release problem by dissolving a significant portion of the undissolved solids thought to be responsible for the waste's gas retention behavior. From the available data, experience, and analyses, it is estimated that a 1:1 dilution of Tank 241-SY-101 waste with a 2 M sodium hydroxide solution will provide this type of *passive* mitigation (Hudson et al. 1995).

Because Tank 241-SY-101 has experienced the largest, most hazardous gas releases, and because its waste is scheduled for early retrieval, it became the target for the initial design considerations for using dilution as a mitigation strategy (Rieck 1993). However, because 241-SY-101 is nearly full, dilution requires transfer of much of the diluted waste to inventory space elsewhere. Through a preliminary analysis of the technical, safety, and operational aspects of this dilution-transfer process, it was decided to plan for an in-tank dilution demonstration in nearby Tank 241-SY-103 to prove the utility of dilution in the mitigation efforts.

As required during pump installation and performance testing in Tank 241-SY-101, the in-tank dilution demonstration required modeling efforts to define an envelope for safe operations (Allemann et al. 1994) . Many of the thermal-hydraulic models developed for the SY-101 efforts have been easily adapted for use with Tank 241-SY-103 (Antoniak 1994). However, dilution introduces the diluent, which is chemically different than the waste, and changes in composition and phase equilibria will certainly occur. Changes in phase equilibria affect the waste rheology significantly through changes in solids content and in the composition of both the liquid and solid phases. These changes, in turn, impact the physics of gas retention, bubble rise, and heat transport, which must be understood to define the safety envelope. Because of the coupling of these processes, modeling the waste transport and gas retention during waste dilution requires integrating current precipitation/dissolution models into the developed thermal-hydraulic tank models.

In addition to the dissolution/precipitation model, improvements to the physical property models were required to more adequately model the waste physics. We have included new or updated physical properties models for supernatant liquid, solid chemical, slurry density, thermal

conductivity, viscosity, and specific heat. New rheology models have been included to describe sludge strength, shear stress, and gas bubble and solid particle drag more adequately. We have also incorporated many of the correlations for physical and rheological properties for density, viscosity, yield strength, surface tension, heat capacity, and solubilities of salts and multi-component systems, as suggested by Mahoney and Trent (1995). And attempts have been made to incorporate parts of the ongoing experimental work of Gauglitz (Mahoney and Trent 1995; Gauglitz et al. 1995; Rassat and Gauglitz 1995) to quantify tensile stress in sludge and the work of Bunker to identify shear stress variation as a function of pH.[a]

Originally, modeling the dilution demonstration in Tank 241-SY-103 was to be completed in two phases–development and application–with the latter being direct support for resolving safety and operational issues. However, late in 1994 a decision was made to defer plans for the in-tank dilution demonstration pending a decision on whether to pursue dilution as a mitigation strategy. As a part of this decision, the application phase of this modeling effort was deferred.

This report documents the progress made in integrating the dilution/precipitation chemistry models into the TEMPEST thermal-hydraulics model and upgrading some of the key physics and physical property models. Brief descriptions of the general TEMPEST code formulations, including constituent transport equations, are presented in Section 1. In Section 2, coupling fast and slow chemical reactions with physical movements is discussed, as is an improved physical property and rheological modeling approach. Two test conditions (decayed jet tank segment and dilution injection) and the detailed results and evaluations of these two model test cases are contained in Section 3. Conclusions derived from the study and recommendations for future studies are presented in Section 4.

## 1.1 Hydrodynamics and Transport: Constituents and Chemical Species

The TEMPEST Code was used to compute transport of chemical species and constituents (solid, liquid, and gaseous phases) within the laws of hydrodynamics. The TEMPEST fluid dynamics computer code (Trent and Eyler 1988) solves the three-dimensional, time-dependent equations of turbulent momentum, heat, and mass transport. It uses the k-ε turbulence model (Rodi 1984) and can accommodate non-Newtonian power law fluids as well as fluids whose viscosity and yield stress depend upon solids concentration. Transport of multiple liquid, gas, and/or solid constituent species can be performed. The thermal energy solution accommodates fully coupled heat transfer in liquids, gases, and solids; surface radiation; and may be coupled to a multi-electrode, multiphase, arbitrary wave form electric field model to consider Joule heating.

TEMPEST uses the integral form of the fundamental conservation laws applied in the finite volume formulation, as cast in Cartesian tensor form:

---

a) Bunker, B. C. 1995. Reported in Tank *Waste Treatment Science: Report for the Second Quarter of FY 1995*, J. P. LaFemina, ed. TWRSPP-95-008, Pacific Northwest Laboratory, Richland, Washington, pp. 76–85.

- Conservation of mass (continuity)

$$\frac{\partial}{\partial t}\int_{cv}\rho dV + \int_{cs}\rho U_s dA_s = 0 \tag{1.1}$$

- Conservation of momentum (Newton's second law)

$$\frac{\partial}{\partial t}\int_{cv}\rho U_r dV + \int_{cs}\left(\rho U_r U_s + j_{\mu_s}\right)dA_s = \dot{S}_m \tag{1.2}$$

- Conservation of energy (1st law of thermodynamics)

$$\frac{\partial}{\partial t}\int_{cv}\rho e dV + \int_{cs}\left(\rho U_s h + j_{qs}\right)dA_s = \dot{S}_q \tag{1.3}$$

- Conservation of turbulent kinetic energy, k

$$\frac{\partial}{\partial t}\int_{cv}\rho k dV + \int_{cs}\left(\rho U_s k + j_{ks}\right)dA_s = \dot{S}_k \tag{1.4}$$

- Conservation of turbulent kinetic energy dissipation, ε

$$\frac{\partial}{\partial t}\int_{cv}\rho \varepsilon dV + \int_{cs}\left(\rho U_s \varepsilon + j_{\varepsilon s}\right)dA_s = \dot{S}_\varepsilon \tag{1.5}$$

- Conservation of mass constituents, $C_i$

$$\frac{\partial}{\partial t}\int_{cv}C_i dV + \int_{cs}\left(U_s C_i + j_{C_i s}\right)dA_s = \dot{S}_{C_i} \tag{1.6}$$

Nomenclature for the tensor quantities in the above conservation laws is as follows:

| | | |
|---|---|---|
| r | = | tensor coordinate index, r = 1, 2, 3 |
| s | = | tensor summation index (used as a free index), s = 1, 2, 3 |
| $X_r$ | = | $r^{th}$ space coordinate |
| $U_r$ | = | velocity component, in the $r^{th}$ coordinate direction |
| $F_r$ | = | force component, in the $r^{th}$ coordinate direction |
| $g_r$ | = | gravitational component, in the $r^{th}$ coordinate direction |
| $A_s$ | = | area, in the s coordinate direction |
| $j_{xs}$ | = | diffusive flux for conserved quantity, x, in the s coordinate direction (μ and g as x are momentum and heat). |

Nomenclature for scalar quantities:

| | |
|---|---|
| $\rho$ | = density |
| $t$ | = time |
| $V$ | = volume |
| $e$ | = internal energy |
| $h$ | = enthalpy |
| $k$ | = turbulent kinetic energy |
| $\varepsilon$ | = turbulent kinetic energy dissipation |
| $C_i$ | = mass concentration, $i^{th}$ constituent (partial density) |
| $\dot{S}_m$ | = source term for momentum |
| $\dot{S}_q$ | = source term for thermal energy |
| $\dot{S}_k$ | = source term for turbulent kinetic energy |
| $\dot{S}_\varepsilon$ | = source term for dissipation of turbulent kinetic energy |
| $\dot{S}_{C_i}$ | = source term for $i^{th}$ mass constituent |

Others: cx, cv = control surface and volume, respectively.

The flux terms $\mathbf{j}_{xs}$ used in TEMPEST are typically gradient functions of the conserved quantity, x. In general, the transport coefficient (e.g., diffusivity or conductivity) for each of these relationships is a tensor quantity that reflects the anisotropic behavior of the transport media. In the conservation of momentum, for example, the term for Stokes viscosity is defined as

$$\mathbf{j}_{\mu_s} = -\mu \frac{\partial U_s}{\partial x_r} \tag{1.7}$$

and for mass diffusion (Fick's law), the flux, $\mathbf{j}_{C_i s}$ is defined as

$$\mathbf{j}_{C_i s} = -D_i \left( \frac{\partial C_i}{\partial x_s} \right) \tag{1.8}$$

where $D_i$ is the diffusion coefficient for the $i^{th}$ constituent.

## 1.2 Chemical Constituent Species Transport

TEMPEST provides for constituent transport in the form of advection, diffusion, and source contributions. The equivalent differential form of the finite volume constituent transport equation solved by TEMPEST is

$$\frac{\partial C_i}{\partial t} + \frac{\partial}{\partial x_s}\left[ \left( U + u_i \right)_s C_i \right] = \frac{\partial}{\partial x_s}\left\{ D_m \frac{\partial C_i}{\partial x_s} \right\} + s_{C_i} \tag{1.9}$$

where

$C_i$ = partial density of the $i^{th}$ constituent
$D_m$ = mass diffusion coefficient of the mixture
$u_i$ = slip velocity of $i^{th}$ constituent
$x_s$ = coordinate in direction s
$s_{C_i}$ = source term for $i^{th}$ constituent

In the TEMPEST finite volume discretization approach, the differential form of the transport equation (Equation 1.9) is interpreted in a finite volume form where constituents are transported from cell to cell. The solutions of the flow field and constituent concentration are performed in a transient fashion. For the dissolution/precipitation chemistry mechanics, the reacting components (aqueous species, dissolved and undissolved solids) are treated as transported components and individually transported. This process occurs at each time step for each cell. A chemical reaction via equilibrium and kinetics modules occurs at the user-specified time points following the solution of the transport equations for all species.

The slip velocity, $u_i$, is calculated by correlation based on the phase and properties of species and a base fluid. Solids, gases, and aqueous species have unique correlation sets available. These correlations and the property effects have been documented in the *TEMPEST T2 Theory Manual* (Trent and Eyler 1994); enhancements to FY 1995 correlation models development conducted by Mahoney and Trent (1995) at PNL are outlined in Section 2.

The transported/reacting process for TEMPEST in hydrodynamic chemistry simulations means that individual species move uniquely, settle if they are heavy solids or rise if they are gases or light solids, or simply move with the velocity of the base liquid if they are aqueous components. The convective base fluid motion is derived from the solution form of the Navier-Stokes equations described above and captures forced flow from jets or streams, or buoyancy induced motion from thermal distortions or density stratification. The chemically reacting species then induce chemical reactions and potential dissolution/precipitation of solids within the representative fluid field.

# 2.0 Technical Approach

In this section, the coupling of fast and slow chemical reactions with physical movements is discussed, followed by a discussion of an improved physical property and rheological modeling approach.

## 2.1 Dissolution And Precipitation Chemistry

### 2.1.1 Objective of Dissolution/Precipitation Modeling

The objective of the dissolution and precipitation modeling effort is to account for the effects of solids dissolution and precipitation on physical properties and rheology, thus to improve the reliability of tank waste simulation by the TEMPEST code. Precipitation and dissolution affect the physical behavior of tank wastes, including

1) gas retention in the sludge layer because of the changes in type, size, and amount of solids that trap gases

2) solid resuspension and settling through changes on densities of supernatant liquid and sludge by solid chemical composition changes

3) convective flow and physical species motions through changing rheology (e.g., viscosity and yield stress/strength) by solid and aqueous chemical composition changes and pH change, and through changing bubble rise velocity and solid particle settling/rising by changing viscosity and drag behind bubbles and solid particles.

Thus precipitation and dissolution were incorporated into the TEMPEST code to more reliably estimate physical properties and rheology and to improve prediction of spatial variations of tank wastes.

Integrating chemical reactions into TEMPEST allows us to predict:

1) dissolution/precipitation such that evolving chemical concentrations are available for estimating physical properties and rheology

2) adsorption/desorption reactions (if applicable) affecting chemical compositions

3) pH and other chemical variables for improved predictions of effective viscosity and other rheology

4) behavior of chemically reactive gas and solid fractions affecting gas retention.

### 2.1.2 Basic Technical Approach

A preliminary TEMPEST modeling simulation was conducted for this study using a pre-assigned single dissolution/precipitation reaction relationship; it confirmed the feasibility of incorporating chemical reactions into TEMPEST to reflect precipitation/dissolution effects on tank waste transport modeling. However, it was obvious that wider and more flexible selections of reacting chemical species and other variables (including pH) are needed to handle complex tank waste compositions that affect physical properties and rheology. This preliminary testing led to an approach of performing interactive simulations for aqueous chemical reactions, dissolution/precipitation, adsorption/desorption, and some gaseous reactions. This interactive chemical reaction modeling approach requires us to handle both very fast (equilibrium) reactions, such as acid-base reactions, and slow kinetic reactions, such as many precipitation/dissolution and redox reactions. Since all chemical reactions are fundamentally kinetic, solving them kinetically is potentially more accurate (Steefel and Lasaga 1994; Steefel and Lichtner 1994). However, some aqueous chemical reactions (e.g., acid-base reactions) can occur within a very small fraction of a second (Snoeyink and Jenkins 1980; Sawyer et al. 1994). Furthermore, the assumption of equilibrium among various aqueous chemical species can significantly reduce a number of independent chemical unknowns in a system, potentially reducing the computational time significantly. Thus we assumed that fast chemical reactions will reach their equilibrium conditions within each computational time step, while slow chemical reactions will be handled through reaction kinetics. The fast and slow chemical reactions are thus solved separately with their interactions.

Fully coupling transport and chemical reactions provides for feedback between chemical reactions and physical transport processes within the same time step. For a groundwater system, this was accomplished by using the global implicit method to solve combined reaction and solute transport simultaneously (Yeh and Tripathi 1989; Steefel and Lasaga 1994). This full coupling allows some important feedback on the groundwater system (e.g., change of porosity due to chemical dissolution/precipitation, affecting the movement of the groundwater and the chemical front, which in turn affect local chemical reactions). However, the full coupling of chemical and physical transport processes requires significantly more computational time compared with an approach of sequentially modeling the transport and chemical reactions. Furthermore, our potential tank simulation time steps are expected to be very small, thus allowing us to assume that the effects of chemical reactions on physical properties and rheology are very small within a small time step. Thus, we selected the approach that chemical transport and reactions are also treated sequential, rather than fully coupled. The modeling sequence within a time step adapted for this study is to

1) simulate flow and transport

2) calculate fast (equilibrium) chemical reactions

3) calculate slow kinetic chemical reactions

4) recalculate fast (equilibrium) chemical reactions

5) calculate physical properties and rheology.

This sequence is repeated in the following time step. Furthermore, to incorporate interactive chemical reaction modeling into TEMPEST, we decided to integrate a working chemistry code into TEMPEST rather than develop a new chemistry code under this study. This chemistry code must be able to handle the high-ionic-strength conditions that occur in the waste tanks.

### 2.1.3 Specific Technical Approach

*Equilibrium Chemical Reactions*: Based on the approach described above, a working equilibrium chemical code was incorporated into the TEMPEST code to simulate fast chemical reactions. We selected the equilibrium chemical code, GMIN (Felmy 1990), for this purpose. The GMIN code calculates the chemical composition of systems composed of aqueous phases, pure solid phases, solid-solution phases, adsorbed phases, and gas phases. In the aqueous phase modeling, the excess solution free energy is modeled by using the Pitzer equations (Harvie et al. 1987), which are valid to high ionic strengths. Thus, GMIN is applicable to tank waste conditions having high ionic strength. The Davies equations (Felmy 1990) can also be used as an option in the GMIN code. The mathematical algorithm in GMIN is based on a constrained minimization of the Gibbs free energy (Snoeyink and Jenkins 1980; Harvie et al. 1987). This approach is more numerically stable and reliably converges to a free energy minimum, compared with more common chemical equilibrium codes based on the mass-action approach (Felmy 1990). In GMIN, the activity coefficients for non-ideal, solid-solution phases are calculated using parameters of a polynomial expansion in mole fraction of the excess free energy of mixing. The free energy of adsorbed phase species is described by the triple-layer, site-binding adsorption model.

The GMIN code is being used to simulate potential chemical reactions relevant to Hanford waste sludge under the Pretreatment Program. Under this program, Hanford tank wastes are to go through a series of pretreatments prior to solidification. Thus the thermodynamic database for GMIN (e.g., standard chemical potentials) and Pitzer ion-interaction parameters relevant to these chemical reactions are steadily being added and/or updated as they become available under the Pretreatment Program.

The TEMPEST code, modified by incorporating GMIN, now has the basic structure to also simulate reactive gases if supplied with the necessary thermodynamic data for relevant chemical reactions. When these databases are implemented into TEMPEST, the code may be able to simulate movements of gases that have chemical reactions, such as the combined physical and chemical behavior of $NH_3$ gas in some Hanford single-shell tanks. The modified code is also capable of producing spatial and temporal distributions of the activity of the hydroxyl ion, {OH-}, which can be related to the local pH value.

*Kinetic Chemical Reactions:* Slow-reacting precipitation/dissolution and redox reactions are handled by a kinetic chemical model. The precipitation/dissolution reaction equations are decoupled (ordinary differential equations) and solved numerically or analytically. The derivation of the TEMPEST kinetic reaction equations is described below.

Assume that a tank has five solids: $NaNO_3(s)$, $NaNO_2(s)$, $Al(OH)_3(s)$, AlOH(s), and $NaAlO_2(s)$. The tank is also assumed to have nine aqueous species, $Na^+$, $(H^+)$, $OH^-$, $NO_3^-$, $NO_2^-$, $Al(OH)_4^-$, $AlO_2^-$, $NaNO_3(aq)$, $NaNO_2(aq)$, and $H_2O$.

Suppose that the following chemical reactions are assumed to occur in a tank:

$$Na^+ + NO_3^- = NaNO_3(aq) \quad (2.1)$$

$$Na^+ + NO_2^- = NaNO_2(aq) \quad (2.2)$$

$$Na^+ + NO_3^- = NaNO_3(s) \quad (2.3)$$

$$Na^+ + NO_2^- = NaNO_2(s) \quad (2.4)$$

$$Na^+ + Al(OH)_4^- = Na^+ + OH^- + Al(OH)_3(s) \quad (2.5)$$

$$Na^+ + Al(OH)_4^- = Na^+ + OH^- + H_2O + AlOOH(s) \quad (2.6)$$

$$Na^+ + Al(OH)_4^- = NaAlO_2 + 2H_2O \quad (2.7)$$

$$Na^+ + AlO_2^- = NaAlO_2(s) \text{ (possibly under very high pH)} \quad (2.8)$$

For the kinetic reactions, we assume the following rate law, R, for solid i (Steefel and Lasaga 1994):

$$R_i = \frac{d[C_{si}]}{dt}$$

or

$$R_i = \{\text{sign of } (\ln \frac{Q_i}{K_i})\}\{k_{i1} + k_{i2}'(\text{solids surface area})\}\{1 - \frac{Q_i}{K_i}\}^{m_i} \quad (2.9)$$

where

| | |
|---|---|
| $[C_{si}]$ | = molality of solid, i |
| $K_i$ | = equilibrium constant |
| $k_{i1}$, $k_{i2}'$ | = kinetic rates of a solid |
| $m_i$ | = constant |
| $Q_i$ | = activity product |

The above kinetic expression can be used for both elementary and non-elementary reaction cases. Now, assume that $m_i = 1$. Because solid surface area per unit weight of water is proportional to the amount of solids per unit weight of water, we simply assumed that

$$\text{solid surface area} = b_{si}[C_{si}] \quad (2.10)$$

where $b_{si}$ = constant. Then the rate law (Equation 2.9) becomes

$$R_i = \frac{d[C_{si}]}{dt} = \{k_{i1} + k_{i2}[C_{si}]\}\{1 - \frac{Q_i}{K_i}\} \quad (2.11)$$

where $k_{i2} = b_{si}k_{i2}'$.

Thus the corresponding rate law for associated aqueous species, $w_j$, is

$$R_{wj} = \frac{d[C_{wj}]}{dt} = a_i\{k_{i1} + k_{i2}[C_{si}]\}\{1 - \frac{Q_i}{K_i}\}$$

$$R_{wj} = a_i \frac{d[C_{si}]}{dt} \quad (2.12)$$

where

$a_i$ = moles of species in one mole of solid
$[C_{wj}]$ = molality of aqueous species, j

For nonzero $k_{i2}$ values, an analytical solution of Equation 2.11 is

$$C_{si} = \frac{\{k_{i1} + k_{i2}C_{s0i}]\exp\{-(1 - \frac{Q_i}{K_i})k_{i2}t\} - k_{i1}\}}{k_{i2}} \quad (2.13)$$

where $C_{s0i}$ = the initial concentration of i-th solid.

When $k_{i2}$ equals zero, the analytical solution of Equation 2.11 becomes

$$C_{si} = -k_{i1}\{1 - \frac{Q_i}{K_i}\}t + C_{s0i} \quad (2.14)$$

Equations 2.12, 2.13, and 2.14 were implemented into TEMPEST to simulate the kinetic chemical reactions. In addition, the Hamming method was implemented into TEMPEST when kinetic reaction equations were expressed by coupled ordinary differential equations. These equations, in general, are coupled nonlinear ordinary differential equations, because $K_i$ and $Q_i$ are functions of all chemical concentrations relevant to precipitation/dissolution of the chemical solid, i.

Values of $K_i$ and $Q_i$ are calculated by the equilibrium chemical modeling portion of the modified TEMPEST. These values are changing with time during the simulation period. If the modified TEMPEST time steps are small, $K_i$ and $Q_i$ may be assumed constant for a certain number of time steps. Under this assumption, which we adapted in this study, Equation 2.11 becomes a set of decoupled ordinary differential equations for each of the precipitation/dissolution reactions and can be solved numerically or analytically (see Equations 2.13 and 2.14).

### 2.1.4 Data Requirements for Dissolution/Precipitation Modeling

Two types of data are required for the precipitation/dissolution chemical modeling. The first type is thermodynamic data for relevant aqueous, solid, and gaseous chemical reactions. Specifically, for all chemically reacting aqueous, solid, and gas species, these data are

- standard chemical potential with temperature
- Pitzer ion-interaction parameters for binary systems
- Pitzer ion-interaction parameters for common ion ternary systems
- Pitzer ion-interaction parameters for neutral species
- parameters (charges of zero and b planes) used for the triple-layer site-binding adsorption model
- Henry's Law constant.

The second type is model input of chemical and physical data for tank conditions. They are

- initial chemical conditions in a waste tank
  - names of potential chemically reactive aqueous, solid, and gaseous species
  - molality and density of solids
  - molality of individual aqueous species or total aqueous species
  - temperature and pressure
- kinetic reaction rates
  - zero-th order kinetic rate, $k_{i1}$
  - the first-order kinetic rate, $k_{i2}$.

## 2.2 Physical Property and Rheological Modeling

Models and correlations for various applicable physical properties and rheological properties have been developed for TEMPEST waste tank simulation (Mahoney and Trent 1995). TEMPEST performs hydrodynamic simulations of flow and heat transfer in non-Newtonian fluids. Transport of solid, gas, and liquid species are accounted for by the TEMPEST mechanics, which are advected with relative velocities to the mean fluid. Rheology models for sludge strength, shear stress, and gas bubble and solid particle drag are incorporated in TEMPEST. Additional work has been performed to support the present study.

The physical property models have two basic templates: 1) total solids concentration dependence and 2) individual chemical species dependence. The generic correlation for density,

for example, is a base constant of supernatant density (called a pseudo-fluid) and a second order polynomial for solids concentration effects. In addition, there is a third-order polynomial modifier for temperature effects. This section outlines the physical property templates and correlations for a supernatant liquid and a solid chemical species, and thermal conductivity, viscosity, specific heat, and density for slurries.

The integration of a dissolution/precipitation chemistry module allows the various phase species concentrations to enter into the rheological calculations that affect the TEMPEST hydrodynamic flow calculations. The yield strength template of non-Newtonian sludge correlates yield to a power function of solids concentration. Likewise, shear stress is concentration-dependent, and the dissolution/precipitation chemistry calculations develop the species concentration evolution that produces fluid resistance changes.

Pseudo-fluid density is determined from correlation to temperature and solids concentration. As a first approximation, the supernatant liquid in Hanford waste tanks can be treated as a single-component solution, using one of the major aqueous species as a surrogate for the rest. The template for such an approach is by

$$\rho_c = a_0 + a_1C + a_2C^3 + a_3T + a_4/T + a_5CT + a_6T^2 \qquad (2.15)$$

where

$a_k$ = coefficients obtained by data correlation
$C$ = total concentration of all solutes in weight percent of the total solution.

Some groundwork has been laid to apply the methodology of aqueous species concentration to the density correlation, as described in Mahoney and Trent (1995). This technique defines pseudo-fluid density as

$$\rho_c = a_0 + a_1C + a_2C^3 + a_3T + a_4/T + a_5CT + a_6T^2 + \sum_{i=1}^{N} b_i m_i \qquad (2.16)$$

where

$a_k$ = coefficients obtained by data correlation
$m_i$ = molality of the i-th of N aqueous species (mol/kg water in solution)
$b_i$ = density coefficient (from correlation) of the i-th aqueous species

Currently, the aqueous species molality is available, so only the correlation or specification of $b_i$ is needed to complete this capability.

Because GMIN uses molality, partial densities of chemically reactive species simulated in TEMPEST are converted to molality using

$$m_i = \frac{C_i}{C_{H2O}} \frac{1000}{W_i} \tag{2.17}$$

where

$C_i$ = weight percent of the i-th aqueous species
$C_{H2O}$ = weight percent of water in the solution = 100 - C
$W_i$ = molecular weight of the i-th aqueous species.

Solid species density is user-defined in the TEMPEST input data set as a constant or temperature-dependent property. Chemically reactive solid species have their densities assigned in a built-in library data set. Liquid-solid-gas slurry densities are computed via the appropriate volume averaging procedures, as outlined in the TEMPEST Theory Manual (Trent and Eyler 1994).

Pseudo-fluid conductivity and specific heat are based on volume averaging individual constituent contributions. The individual constituent property is correlated to temperature. Pseudo-fluid viscosity is correlated to the fluid viscosity with modification based on the aggregate solids concentration. The fluid viscosity may be taken from a library of pure fluids, say water, or may be initialized by the user as a polynomial function of temperature during input data specification.

Non-Newtonian shear stress models consist of a generic model, as outlined by the TEMPEST theory Manual (Trent and Eyler 1994). These models have provisions for a Bingham model correlated against Hanford waste data. Here the shear stress is defined by

$$\tau = -\left\{\eta_0 + \frac{\tau_0}{\left|\sqrt{\frac{1}{2}\Pi_D}\right|}\right\}\mathbf{D} \qquad \text{for} \quad \tfrac{1}{2}\Pi_D > \tau_0^2 \tag{2.18}$$

and

$$\mathbf{D} = 0 \qquad \text{for} \quad \frac{1}{2}\Pi_D < \tau_0^2$$

where

$\mathbf{D}$ = shear rate tensor
$\Pi_D$ = second invariant of the shear rate tensor
$\tau_0$ = yield strength
$\eta_0$ = Newtonian viscosity at very low shear rate

The correlations for $\tau_0$ and $\eta_0$ are

$$\tau_0 = \tau_{ns} (C_r + a_1(C_r)^{a_2}) \tag{2.19}$$

$$\eta_0 = \eta_{ps}(1 + a_3(C_r)^{a_4}) \tag{2.20}$$

Gas constituents are defined as groups of bubbles of specified sizes (diameters). The relative velocity for bubbles can be modeled by various correlations—simplified buoyant bubble Wallis model (Trent and Eyler 1994), Wallis multiple regime model, or Fan and Tsuchiya model (Mahoney and Trent 1995). Solid particle models include specified settling, hindered settling (Trent and Eyler 1994), or a multiple Wallis regime model, based on specified particle sizes. This last model is a variant of the spherical bubble model for gas bubbles. Aqueous species and dissolved solids have no relative (slip) velocities but move with the pseudo-fluid.

Relative motion of solid and gas constituents produces forces on the pseudo-fluid (restraining in the case of opposite direction motion or driving in the case of similar direction motion). These forces are accounted for in the form of relative drag of the aggregate constituents on the pseudo-fluid. Each constituent can possess individual relative motion, so the absolute drag is the vector sum of the relative forces. The drag is computed for solid particles and gas bubbles based on equivalent drag coefficients derived from the relative velocity models.

The total drag of the bubbles or particles on the fluid (and vice versa) associated with a cell is

$$D = \sum_{N_b} C_d A_c \left\{ \tfrac{1}{2} \rho_b v_s^2 \right\} = \sum_{N_b} \left[ C_d \, N_b (\pi r_b^2) \, \tfrac{1}{2} \rho_b v_s^2 \right] \tag{2.21}$$

where

$r_s$ = bubble/particle effective radius
$N_b$ = the number of bubbles in a cell
$V_s$ = particle relative velocity
$C_d$ = drag coefficient based on cross sectional area
$\rho_b$ = bubble/particle density

and

$$N_b = \frac{3}{4\pi r_b^3} (\text{cell volume}) \, \varepsilon_{d,species} \tag{2.22}$$

where

$\varepsilon_{d,species}$ = volume fraction

The analyses that follow in Section 3 demonstrate the enhanced TEMPEST capabilities and examine the coupling of the dissolution/precipitation chemistry and rheology processes.

# 3.0 Model Applications

When a waste in one tank is mixed with wastes in other tanks or fluids, aqueous and possibly dissolution/precipitation reactions will occur to respond to the new condition. The solids dissolution and precipitation change solid and aqueous (and possibly gaseous) chemical composition, including pH, and thus affect physical properties (e.g., densities of supernatant liquid and sludges), rheology (e.g., viscosity and yield stress/strength), and flow conditions (e.g., drags behind bubble and solid particles), as discussed in Section 2. These changes can, in turn, affect the physical behavior of tank wastes, including gas retention in the sludge layer, solids resuspension and settling, and convective flow and physical species motions. Because some waste tank operations potentially mix waste streams and solutions, various chemical reactions can take place under these operations. The modified TEMPEST, coupling physical transport and chemical reactions, is useful for analyzing various waste tank operations in which both the physical movements and chemical reactions of wastes must be considered. These cases include in-line dilution of wastes by some solutions, in-tank waste dilution, and some pretreatment activities.

Because TEMPEST was modified to account for 1) fast equilibrium chemistry, 2) slow kinetic chemistry, and 3) some associated changes in physical properties and rheology, a series of relatively simple tests was conducted to 1) check if these modifications were implemented correctly, 2) evaluate the behavior of the modified TEMPEST under different conditions, and 3) examine the potential for the code to be used for the tank waste dilution analysis.

## 3.1 Test Conditions and Modeling Results Summary

We selected two sets of geometric and physical conditions that are simple but still resemble the basic physical and chemical conditions of some portions of a waste tank receiving a jet injection. The first set (the decayed jet tank segment model) is a two-dimensional flow field resembling a portion of the tank away from the jet injection point. The main objective of this set was to clearly discern the effects of chemical reactions on constituent concentrations, as predicted by the modified TEMPEST. To achieve this objective, we selected this set to have a flow field such that the physical mixing achieves almost complete mixing in the study tank segment within a simulation time. In this way, the effects of chemical reactions can be clearly examined. The second set (the dilution injection model) also has a two-dimensional (axisymmetric) flow field that resembles an area in the immediate vicinity of the jet injection point in a waste tank. The second set has a more complex flow field that is closer to the flow field expected under actual tank dilution operations.

We assumed that the jet contained only water to enhance the dissolution of the reactive solids. Both sets were assumed to contain 11 constituents (four solids, six aqueous species, and a gas mixture). To simplify model test cases, $NH_3$, $N_2O$, gibbsite, boehmite, and others were not included in the modeling. The solids in these test cases are represented by chemically reactive $NaNO_3$(s), $NaNO_2$(s), and two other nonreactive solids. Aqueous species were $H_2O$, $Na^+$, $NO_3^-$, $NO_2^-$, $NaNO_3$(aq), and $NaNO_2$(aq), as supernatant liquid. A gas species is a hydrogen and nitrogen mixture and treated as a nonreacting species.

We tested and compared the model results, incorporating varying degrees of chemical reactions. Each of these two sets consisted of

- a case with only physical mixing without chemical reactions
- a case with physical mixing, and chemical equilibrium reactions but without kinetics
- cases with physical mixing, chemical equilibrium ,and kinetic reactions.

These cases will be discussed below in more detail.

### 3.1.1 Decayed Jet Tank Segment Model Set

The purpose of this portion of model testing was to examine how TEMPEST predicts the potential effects of chemical reactions on the flow and constituent concentrations approaching the stage of the complete mixing and chemical equilibrium conditions, as stated above. For this purpose, we selected the test setup to simulate a short burst from a radial jet of pure water into a simulated cylindrical tank segment region containing sludge, as shown in Figure 3.1.

The model is an axisymmetric two-dimensional representation of the cylindrical tank. The model encompasses a cylindrical region with a 1.55-m radius and 3.16-m height. The injection slot is located 3 in. (0.0762 m) above the tank bottom. For continuity, an outflow region is prescribed some distance above the jet injection point. Pure water was injected horizontally for one second at a velocity of 15 m/sec. At the end of the jet injection, the dilution had reduced the average species concentration by about 30%, and the tank segment was sealed. The jet induced a recirculating flow pattern, mixing the diluent and tank constituents long after the jet injection ceased; thus we approached a completely mixed, equilibrium concentration distribution. Because this simulation involved a confined heterogeneous mixture at one second into the transient, comparative states for solids dilution with chemical reactions were readily tracked.

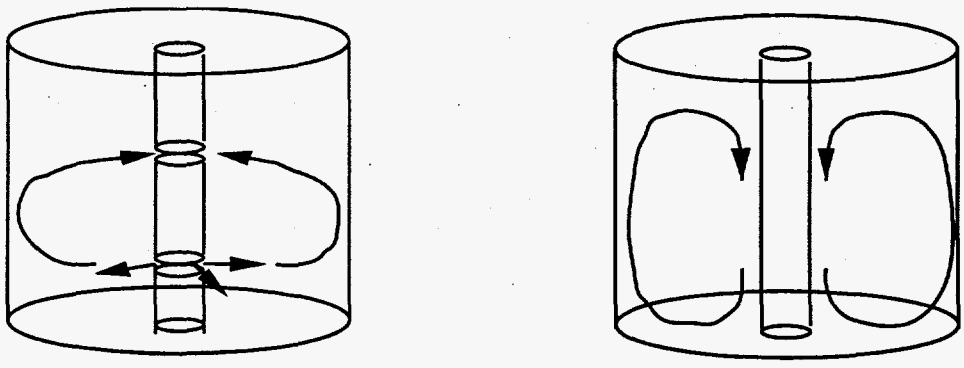

Initial, one-second Jet Circulation

Jet Decay Recirculation

**Figure 3.1.** Decayed Jet Tank Segment Model

*Initial Conditions*: The initial concentrations were composed so that the solution was in equilibrium conditions with $NaNO_3(s)$ and $NaNO_2(s)$. Table 3.1 lists the initial species concentrations. These same concentrations were also used for the dilution injection case.

The initial conditions for nitrate and nitrite components shown in the table are higher than those reported for Tank 241-SY-101 (Reynolds and Herting 1984; Tank Waste Science Panel 1991). The solubilities of $NaNO_3(s)$ and $NANO_2(s)$ are known to be sensitive to both NaOH and temperature (Reynolds and Herting 1984). For simplicity, we did not include NaOH in our current testing, and the temperature was assumed to be 25°C. These conditions partially account for initial conditions that were somewhat different from those expected in Tank 241-SY-101. Our preliminary testing revealed that inclusion of NaOH and $Al(OH)_4^-$ in the modeling reduces solubility limits of $NaNO_3(s)$ and $NaNO_2(s)$. We plan to include these additional aqueous species in future model testing and applications.

Some vertical variations in nonreacting solids were introduced to generate initial depth-varying yield strength. The resulting average density of the sludge was about 1730 kg/m$^3$ at the lowest 10% depth and about 1550 kg/m$^3$ over the rest of the region. Based on the Hanford Tank concentration-dependent correlations, the sludge yield strength was estimated to be 48 Pa and 23 Pa in the lowest 10% and the rest of the tank, respectively. Physical and rheological properties are affected by the species, especially by solid concentrations. This analysis employs the tank correlation yield stress modeling, a Bingham shear stress model, and the Wallis particle drag models outlined in Section 2.2.

*Test Cases*: We ran five cases to evaluate how the modified TEMPEST predicts the effects of solid dissolution/precipitation on physical properties and rheology, which, in turn, affect velocity and constituent distributions. Three (Cases 1 through 3) of the five cases incorporate

**Table 3.1.** Initial Concentrations for Decayed Jet Tank Segment and Dilution Injection Models

| Species | Concentration kg/m$^3$ | Molality |
|---|---|---|
| $NaNO_3(s)$ | 430 | 12.7 |
| $NaNO_2(s)$ | 398 | 14.5 |
| $Na^+$ | 117 | 13.0 |
| $NO_3^-$ | 137 | 5.57 |
| $NO_2^-$ | 133 | 7.43 |
| $NaNO_3(aq)$ | 38 | 1.11 |
| $NaNO_2(aq)$ | 87 | 3.04 |

physical mixing, chemical equilibrium, and kinetic reactions. The fourth case (Case 4) is a combination of physical mixing and chemical equilibrium reactions without kinetic reactions. The last case (Case 5) is with physical mixing only. The five cases are summarized below.

1) Physical mixing, fast (equilibrium), and slow (kinetic) chemical reactions with kinetic rates of $k_1 = 0$ and $k_2 = 0.003$/sec (see Equation 2.12) for $NaNO_3(s)$ and $NaNO_2(s)$

2) Physical mixing, fast (equilibrium), and slow (kinetic) chemical reactions with kinetic rates of $k_1 = 0$ and $k_2 = 0.001$/sec for $NaNO_3(s)$ and $NaNO_2(s)$

3) Physical mixing, fast (equilibrium), and very slow (kinetic) chemical reactions with kinetic rates of $k_1 = 0$ and $k_2 = 1 \times 10^{-6}$/sec for $NaNO_3(s)$ and $NaNO_2(s)$

4) Physical mixing and only fast (equilibrium) chemical reactions without kinetic reactions

5) Physical mixing only without any chemical reactions.

*Summary of Results*: We ran the modified TEMPEST for 15 minutes simulation time for Cases 1 through 3 to examine slowly occurring $NaNO_3(s)$ and $NaNO_2(s)$ dissolution/precipitation impacts. For Cases 4 and 5, we ran it for 100 seconds. The time steps were varied during these simulations; the average time step was approximately 10 milliseconds. The following is a summary of the results of these five cases:

- Case 1 was set up to check overall chemical reaction calculations and procedures, in particular, the kinetic reaction algorithm. Case 1 is a relatively realistic kinetic reaction (faster end of the expected rate change) and, along with Case 2, shows the most realistic simulations among the five cases. This case shows the reactive solids of $NaNO_3(s)$ and $NaNO_2(s)$ continuously dissolving and thus increasing all the aqueous species concentrations with time. Still, the supernatant liquid is unsaturated with solids over the 15-minute simulation time. These chemical changes are also influencing supernatant and composite sludge densities and viscosity and shear /yield stress values, thus affecting the flow field and constituents transport.

- Case 2 was also set up to check the chemical calculations, particularly the kinetic reactions. Similar to Case 1, this case also has a relatively realistic kinetic rate (the slower end of the expected rate change). Although the dissolution of $NaNO_3(s)$ and $NaNO_2(s)$ is occurring with time because of this case's slower kinetic rate, solid and aqueous chemical conditions are farther away from the ultimate equilibrium conditions than those of Case 1. This slower dissolution reaction has fewer impacts on physical properties and rheology.

- Case 3 also has both equilibrium and kinetic reactions taking active roles. This case has a very small kinetic rate term, and was set up to further examine the kinetic reaction calculations and compare them with the results of Cases 1 and 2. These three

cases constitute the sensitivity analysis for the solids dissolution/precipitation reactions. Because there is hardly any solids dissolution occurring in this case, the supernatant liquid diluted by the pure water jet is more unsaturated with $NaNO_3(s)$ and $NaNO_2(s)$ than Cases 1 and 2 and has the highest reactive solid concentrations. Comparing these three cases clearly reveals the effects of solid dissolution on physical properties and rheology (e.g., the yield stresses are generally lower in Case 1 than in Case 2, which are lower than those in Case 3). These property and rheologic changes affected the predicted movements of waste constituents in the tank.

- Case 4 was set up to examine equilibrium calculation procedures and results. Because Case 4 has instantaneous dissolution of $NaNO_3(s)$ and $NaNO_2(s)$, both reactive solids and all the aqueous species were in equilibrium during the simulations. Thus, this case is not very realistic but constitutes a bounding case to compare with more realistic results of Cases 1 and 2. Case 4 produces the greatest amount of aqueous species concentrations and the least amount of $NaNO_3(s)$ and $NaNO_2(s)$ under the conditions tested. The results of this case correspond to those that will be achieved after a long duration.

- Case 5 does not have any chemical reactions; thus this case may be regarded as a base case for comparisons of species concentrations and rheological changes. Because there is no dissolution of $NaNO_3(s)$ and $NaNO_2(s)$ for this case, the solids concentrations are similar to those of Case 3. However, concentrations of individual aqueous chemical species are different in the two cases; in Case 3 aqueous reactions occur, while in Case 5 they do not.

These simple test cases showed that the modified TEMPEST code simulated tank waste movements with both aqueous and solid dissolution reactions in a predictable manner. Furthermore, TEMPEST demonstrated that these chemical reactions affect physical properties and rheology. These changes in turn affect the movements and distributions of flow in the tank.

### 3.1.2 Dilution Injection Model

In the dilution injection portion of the modeling, the modified TEMPEST was used to analyze a local detail of the dilution injection region, again with a varying degree of chemical reactions incorporated in the analysis. The dilution injection analysis is for demonstration and does not attempt to develop a complete long-term tank injection scenario. The dilution injection model is a two-dimensional axisymmetric, localized representation of a pure water injection into a sludge region, as shown in Figures 3.2 and 3.3. The injection pipe is modeled at the center of the geometry and continuously injects water at 15 m/s down into a sludge region that has the reacting and nonreacting species. The model encompasses a cylindrical region with a 1.55-m radius and 3.37-m height. The injection pipe diameter is 2 inches (0.0508 m), and the injection point is about 0.6 m above the tank bottom. The exterior surfaces of the model were assumed to be impervious to simplify the calculations. An outflow region was modeled at the top surface, although a solid obstruction was placed over most of an outer portion of the surface to eliminate any short-circuit siphoning effect (a flow is drawn into the model area from the top surface and is immediately discharged out from the surface).

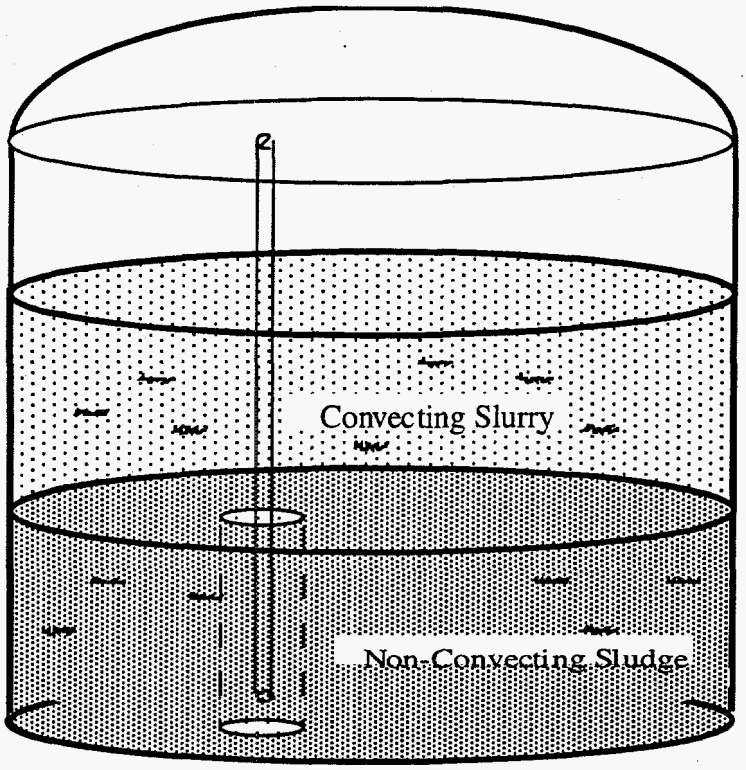


**Figure 3.2.** Waste Tank Dilution Injection Model

*Test Cases*: For the dilution injection model, we also ran five cases to comparatively model results for the effects of dissolution/precipitation on distributions of velocity and constituents. Three (Cases 1, 2, and 3) of the five cases incorporate physical mixing, chemical equilibrium, and kinetic reactions in the analysis, as listed below. The fourth (Case 4) uses physical mixing and equilibrium chemical reaction but no kinetic reactions. The last case (Case 5) uses physical mixing only. Similar to the decayed jet tank segment model discussed previously, the five cases are

1) Physical mixing, fast (equilibrium), and slow (kinetic) chemical reactions with kinetic rates of $k_1 = 0$ and $k_2 = 0.003$/sec (see Equation 12) for $NaNO_3(s)$ and $NaNO_2(s)$

2) Physical mixing, fast (equilibrium), and slow (kinetic) chemical reactions with kinetic rates of $k_1 = 0$ and $k_2 = 0.001$/sec for $NaNO_3(s)$ and $NaNO_2(s)$

3) Physical mixing, fast (equilibrium) and very slow (kinetic) chemical reactions with kinetic rates of $k_1 = 0$ and $k_2 = 1 \times 10^{-6}$/sec for $NaNO_3(s)$ and $NaNO_2(s)$

4) Physical mixing and fast (equilibrium) chemical reactions without kinetic reactions

5) Physical mixing only without any chemical reactions.

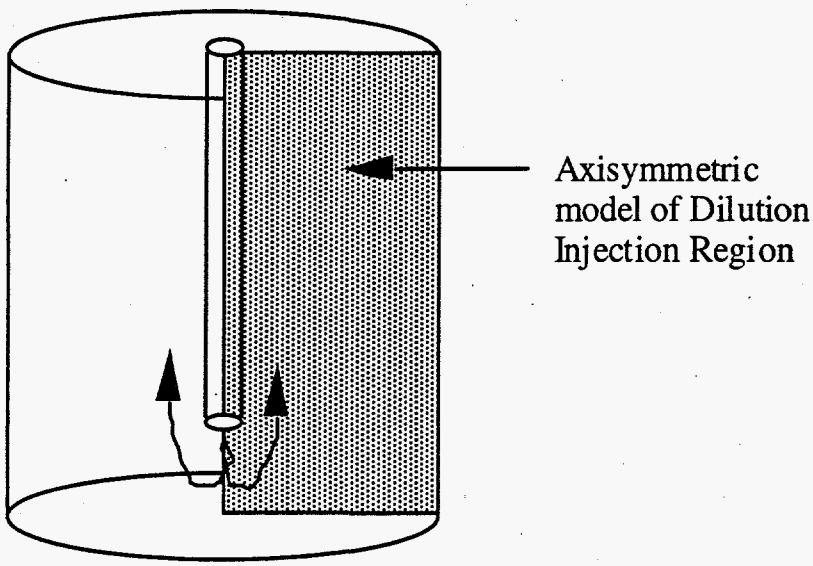


**Figure 3.3.** Dilution Injection Model Region

Conditions of these five cases are identical to Cases 1 through 5 of the decayed jet tank segment model. Thus, similar to the decayed jet tank segment model cases, Cases 1 through 4 were used for examining the algorithms and procedures for the chemical reaction calculations, while Case 5 is a base case without chemistry.

*Results Summary*: We ran the modified TEMPEST for 15 simulated minutes for Cases 1 and 3 to examine slowly occurring $NaNO_3(s)$ and $NaNO_2(s)$ dissolution/precipitation impacts. We ran Cases 4 and 5 for 100 seconds simulation time. Although time steps were changing during these simulations, average time steps were approximately 2 milliseconds. The following summarizes results for these five cases:

- Case 1 was set up to check overall chemical reaction calculations and procedures, in particular, the kinetic reaction algorithm under the more realistic tank injection physical setup. Case 1 is a relatively realistic kinetic reaction case, thus together with Case 2 results is the most realistic simulation of the five. Similar to Case 1 of the decayed jet tank segment model, this case shows the reactive solids of $NaNO_3(s)$ and $NaNO_2(s)$ continuously dissolving over 15 minutes, providing positive contributions to the aqueous species concentrations with time. However, concentrations of all constituents are decreasing with time because of the continuous dilution by pure water jet. These chemical changes have some effects on supernatant liquid and composite sludge densities and viscosity and shear/yield stress values.

- Case 2 was also set up to check the chemical calculations, particularly for the kinetic reactions. Similar to Case 1, this case also has a relatively realistic kinetic rate (the slower end of the expected rate change). Although the dissolution of $NaNO_3(s)$ and $NaNO_2(s)$ is occurring with time because of the slower kinetic rate, solids dissolution and reduction of reactive solid concentrations are less than in Case 1. This slower dissolution reaction has fewer impacts on physical properties and rheology.

- Case 3 also has equilibrium and kinetic reactions taking place, but the kinetic rate term is very small. Cases 1 through 3 constitute the sensitivity analysis for the solids dissolution/ precipitation reactions. Because there is hardly any solids dissolution occurring in this case, the supernatant liquid diluted by the pure water jet is the most unsaturated with $NaNO_3(s)$ and $NaNO_2(s)$, whose concentrations remain relatively high.

- Case 4 was set up to examine equilibrium calculation procedures and results. Because Case 4 has instantaneous dissolution of $NaNO_3(s)$ and $NaNO_2(s)$, both reactive solids and all the aqueous species were in equilibrium conditions throughout the simulations. Thus this case is not very realistic. This case may still constitute an interesting bounding case, but because the buoyant jet rises quickly along the pipe even after a long time simulation (Case 1), the cases with kinetic reactions (Cases 1 through 3) may not necessarily converge to the results calculated by Case 4 until the tank is completely mixed.

- Case 5 does not have any chemical reactions, so this case may be regarded as a base case for comparisons of species concentrations and rheological changes. Even though solids concentrations are similar in Cases 3 and 5, aqueous chemical concentrations are not.

Similar to the decayed jet tank segment model results, the model also reveals some effects of chemical reactions on physical properties and rheology, although these effects are more difficult to discern under the conditions tested here. These cases also reveal a possibility of not reaching an equilibrium condition even with a large amount of time because of the ever-changing conditions occurring in the tank. This leads to potential needs to assess tank chemistry and physics in both disturbed and undisturbed (natural) tank conditions. These tests show that the modified TEMPEST can be useful for addressing complex conditions in which physical movements and chemical reactions affect each other.

## 3.2 Detailed Decayed Jet Tank Segment Model Results and Evaluations

We ran the five cases with and without chemical reactions to 1) check the TEMPEST modifications of equilibrium and kinetic chemical reactions and associated physical properties and rheology, 2) evaluate the behavior of the modified code, 3) examine the potential for the code to be used for the tank waste dilution analysis.

As we described in Section 3.1, Cases 1 through 3 incorporated physical mixing, chemical equilibrium, and kinetic reactions. Case 4 included only physical mixing and equilibrium chemical reactions without including kinetic reactions, and Case 5 incorporated only physical mixing without any chemical reactions being considered. All these cases had an initial burst of jet flow injected into a tank, as shown in Figure 3.4, depicting very early (0.4 seconds) predicted $NaNO_3(s)$ concentrations (volume fractions) for Case 5 (physical mixing only).

We ran Cases 1 through 3 for 15 minutes and Cases 4 and 5 for 100 seconds simulation times. Because the chemical simulation currently requires about two orders of magnitude more computational time than hydrodynamic and transport simulations do, we simulated both the chemical equilibrium and kinetic reactions for only once per hundred time steps for all simulation cases in this study. Note that because the simulation time steps were about 10 milliseconds for the decayed jet tank segment runs, chemistry was still simulated for approximately every second. We also ran Cases 1 through 3 for 10 seconds simulation time with both transport and chemical reactions simulated at every time step to evaluate the effects of not updating chemistry at every time step.

We now present some of the predicted results for these five cases, followed by their evaluations. Figures 3.4 through 3.40 have been placed at the end of Section 3 for easier reading (pp. 3.17 through 3.35).

### 3.2.1 Results of the Decayed Jet Tank Segment Model Runs

For Case 1 (physical mixing and chemistry with the kinetic rate of $k_2 = 0.003/s$), Figure 3.5 shows predicted time-varying volume fractions of reactive solids of $NaNO_3(s)$ at two different locations (Location 1 and 4) over 15 minutes, and the corresponding values of $NaNO_2(s)$ at location 1. Location 1 is approximately 0.58 m from the tank center and 1.58 m above the tank bottom. Location 4 is 1.1 m from the center and 0.33 m above the tank bottom. Figure 3.6 presents predicted time-varying distributions of two nonreactive solids and $H_2/N_2$ gases at location 1 over 15 minutes for comparisons with reactive solid distributions. Figure 3.7 presents its variation over 10 seconds at location 1 when the chemistry simulation was performed at each time step. Predicted spatial distributions of the reactive $NaNO_3(s)$ are presented in Figures 3.8 and 3.9 at one and 15 minutes, respectively, while Figure 3.10 shows the corresponding distribution of reactive $NaNO_2(s)$ at 15 minutes. The predicted velocity distribution at 15 minutes is shown in Figure 3.11.

The temporal variation of predicted $NaNO_3(s)$ distribution over 15 minutes is shown for Case 2 (physical mixing and chemistry with the kinetic rate of $k_2 = 0.001/sec$) in Figure 3.12, while Figures 3.13 and 3.14 depict their calculated spatial distributions at 1 and 15 minutes, respectively. The predicted velocity distribution at 15 minutes is presented in Figure 3.15.

Similarly, Figure 3.16 shows the temporal variations of predicted $NaNO_3(s)$ over 15 minutes for Cases 1 through 3, while Figures 3.17 and 3.18 depict calculated spatial distribution of $NaNO_3(s)$ at 1 and 15 minutes, respectively, for Case 3. Figure 3.19 presents the predicted velocity distributions at 15 minutes for Case 3 (physical mixing and chemistry with the kinetic rate of $k_2 = 1 \times 10^{-6}/s$).

For Case 4 (physical mixing and equilibrium chemistry without kinetic reactions), the calculated temporal variation of $NaNO_3(s)$ volume fractions over 1 minute is shown in Figure 3.20, while its spatial variations at 30 seconds and 1 minute are shown in Figures 3.21 and 3.22.

For Case 5 (physical mixing only without chemical reactions), Figure 3.23 presents the predicted spatial variation of $NaNO_3(s)$ volume fractions at 30 seconds.

### 3.2.2 Evaluations of the Decayed Jet Tank Segment Model Runs

The modified TEMPEST predicted distributions of 11 constituents, two reactive solids ($NaNO_3[s]$ and $NaNO_2[s]$) two similar but nonreactive solids, $H_2/N_2$ gas, $H_2O$, and five aqueous chemical species [i.e., $Na^+$, $NO_3$, $NO_2^-$, $NaNO_3(aq)$, $NaNO_2(aq)$] by accounting for

- fast aqueous equilibrium chemical reactions
- slow kinetic reactions of the solid dissolution
- associated changes on some physical properties and rheology.

This is demonstrated by examining temporal variations of predicted distributions of 11 constituents at various locations over 15 minutes. For example, in Case 1, temporal variations of predicted volume fraction distributions of both $NaNO_3(s)$ and $NaNO_2(s)$ over 15 minutes are decreasing to approximately 0.09 and 0.075, as shown in Figure 3.5. These concentrations are in equilibrium conditions; at the end of 15 minutes, these concentrations are approaching their equilibrium value. Because the kinetic reaction time for $NaNO_3(s)$ and $NaNO_2(s)$ is expected to be roughly between 15 minutes and one hour, Case 1 corresponds to the faster end of the expected kinetic reaction rate of this solid. In contrast, concentrations of nonreactive solids and $H_2/N_2$ gas remained constant over time, except for the first tenths of seconds when the initial dilution of roughly 30% and subsequent physical mixing occurred due to the initial burst of pure water jet injection (see Figure 3.6). The comparisons of these reactive and nonreactive constituents clearly show that the modified TEMPEST predicted chemical reactions in addition to the physical mixing.

These figures also show very rapid variations of the volume fractions at the very early time of approximately 10 seconds. Through the detailed examination of the model results, we confirmed that these rapid variations are mostly due to the physical mixing caused by the initial burst of the pure water jet injection and are not due to computational problems such as numerical instability. Figure 3.7 shows a volume fraction of $NaNO_3(s)$ at location 1 obtained for the 10-second run with the chemistry simulated at every time step. As revealed by the figure, the most rapid variations occur within the first 2 seconds. These variations are due to the pure-water jet hitting location 1 within the first 2 seconds, suddenly reducing the amount of $NaNO_3(s)$ at this location. The subsequent flow circulation induced by the jet brought less disturbed $NaNO_3(s)$ to this location, increasing volume fractions during the next tenths of seconds. However, because the dilution of aqueous species by the pure water makes nitrate and nitrite unsaturated, the kinetic reactions occur to dissolve $NaNO_3(s)$ gradually.

Comparing the 10-second run with the 15-minute run shows that when the chemical equilibrium and kinetic (solid dissolution) reactions were calculated at each time step (approximately every 10 milliseconds), predicted $NaNO_3(s)$ concentrations at 10 seconds were approximately 5% lower than the concentrations when the chemical reactions were simulated for approximately every second. Note that for the latter case, the solids dissolution was still occurring between each second as well. This comparison shows minor differences between predicted results caused by the different frequency of the chemistry simulation. This effect should be further evaluated to select the optimal frequency of the chemistry simulation. Moreover, because the chemical simulations currently require significantly more computational time than hydrodynamic and transport simulations , more efficient computational methods must be implemented into TEMPEST. These include improving the equilibrium chemistry computational method and possibly adapting the parallel processing computational method. Because the chemical reactions themselves are location-independent, the adaptation of the parallel processing for the chemical reaction simulation portion of the code seems to be a very logical step to take.

The kinetic effects on chemical concentrations were also clearly demonstrated by the modified TEMPEST code as shown in Figure 3.16 as well as in Figures 3.9, 3.14, and 3.18 of Cases 1, 2, and 3, respectively. The model predicted that the smaller the values of the kinetic rate term, $k_2$, the slower the dissolution/precipitation reactions and the greater the reactive solid concentrations. For Case 2 with the smaller $k_2$ value of 0.001 per second, the volume fraction of $NaNO_3(s)$ at the end of 15 minutes is approximately 0.11 (see Figures 3.14 and 3.16), compared with 0.094 for Case 1 with a $k_2$ value of 0.003/s (see Figures 3.9 and 3.16). With the rate of 0.001/s, it would take approximately one hour to reach equilibrium for $NaNO_3(s)$; in Case 1, it took approximately 15 to 20 minutes to reach equilibrium. Thus the dissolution of Case 2 constitutes the slower end of the range of realistic dissolution rates of $NaNO_3(s)$ and $NaNO_2(s)$. With the very small kinetic rate of $1 \times 10^{-6}$/s in Case 3 (see Figures 3.16 and 3.18), the kinetic reactions are too slow to have much impact on dissolution/precipitation of $NaNO_3(s)$ and $NaNO_2(s)$ during the 15-minute simulation period. This is shown in Figure 3.16, which reveals constant $NaNO_3(s)$ concentrations over time, except for the initial mixing period in Case 3 ($k_2 = 1 \times 10^{-6}$/s. Note that distributions of the nonreactive solids and gases were identical in Cases 1 through 3, as expected. These tests further confirm that the modified TEMPEST is reproducing the expected trend of the chemical concentrations with solid dissolution/precipitation reactions.

Case 4 (physical mixing and equilibrium chemistry) is another extreme case where all reactions including dissolution/precipitation would occur instantaneously. In our actual modeling run, instantaneous means that all chemical reactions will reach their equilibrium conditions within approximately one second, although the equilibrium conditions themselves keep changing with the results of physical mixing. Because the dissolution/precipitation of $NaNO_3(s)$ and $NaNO_2(s)$ in Tank 241-SY-101 is expected to occur in approximately 15 minutes to one hour, this case is obviously not very realistic. However, the comparison of Case 4 with kinetic condition cases (Cases 1 through 3) confirmed that the equilibrium case may serve as one of the bounding cases, at least for the decayed jet tank segment model. The predicted temporal and spatial variations of $NaNO_3(s)$ and $NaNO_2(s)$ concentrations for Case 4 are the smallest among all cases tested (see Figures 3.8, 3.13, 3.17, and 3.22). Examples are also shown in Figures 3.5 and 3.7 for

Case 1 (with a dissolution kinetic rate of 0.003/s) and Figure 3.20 for Case 4. The volume fraction of $NaNO_3(s)$ at 10 and 60 seconds with the kinetic reactions (Case 1) is approximately 0.13, while with instantaneous dissolution (Case 4) the volume fraction is approximately 0.1.

Because of the continuous dissolution of the reactive solids over time, aqueous species concentrations were changed as well. The simulation results by the modified TEMPEST indicated that the greater the dissolution rates (i.e., $k_2$ values), the smaller the solids concentrations and the larger the aqueous concentrations. This is shown in Table 3.2, presenting predicted representative chemical concentrations at 15 minutes for Cases 1 through 3 and at 30 seconds for Case 4, revealing interaction of the solids and aqueous species. These concentrations were approximately 1.17 m from the tank center and 1.21 m above the tank bottom. Note that the concentrations were reduced by approximately 30% from the initial concentrations through the initial burst of pure water injection for one second. Due to the jet injection and chemical reactions, the mean overall density has decreased and the average concentration of water has increased (e.g., from approximately 400 $kg/m^3$ to 570 $kg/m^3$ for Case 4).

In Case 5 (physical mixing only with neither fast equilibrium nor slow kinetic reactions occurring), $NaNO_3(s)$ and $NaNO_2$ behaved as chemically nonreactive. Thus the model results indicated that this constitutes another bounding case for the decayed jet tank segment model. Because $NaNO_3(s)$ and $NaNO_2(s)$ in the other four cases are dissolving, the case with only physical mixing has the highest concentrations of $NaNO_3(s)$ and $NaNO_2(s)$, as revealed by comparing the predicted $NaNO_3(s)$ concentrations of two bounding cases (Cases 4 and 5) shown in Figures 3.21 and 3.23. Because there is no solids dissolution, Case 5 has the lowest concentrations of aqueous chemical species. Note that Case 3 has different aqueous chemical species distributions

**Table 3.2.** Predicted Chemical Concentrations ($kg/m^3$) at 15 Minutes for Cases 1, 2, and 3 and at 30 Seconds for Case 4 of the Decayed Jet Tank Segment Model

| Chemical Species | Initial Concentration ($kg/m^3$) | Case 1 Faster Kinetics Concentration ($kg/m^3$) | Case 2 Slower Kinetics Concentration ($kg/m^3$) | Case 3 Very Slow Kinetics Concentration ($kg/m^3$) | Case 4 Equilibrium Concentration ($kg/m^3$) |
|---|---|---|---|---|---|
| $NaNO_3(s)$ | 430 | 215 | 248 | 328 | 183 |
| $NaNO_2(s)$ | 398 | 168 | 211 | 304 | 126 |
| $Na^+$ | 117 | 149 | 133 | 97 | 180 |
| $NO_3^-$ | 137 | 176 | 157 | 110 | 193 |
| $NO_2^-$ | 133 | 167 | 149 | 112 | 172 |
| $NaNO_3(aq)$ | 38 | 45 | 38 | 22 | 50 |
| $NaNO_2(aq)$ | 87 | 107 | 90 | 52 | 118 |

than Case 5; in Case 3, aqueous chemical reactions are still occurring, but their effects on reactive solids of $NaNO_3(s)$ and $NaNO_2(s)$ were hardly apparent with the very low kinetic rate. The predicted $NaNO_3(s)$ volume fraction due to the physical mixing alone is about 14%, compared with about 10% under chemical equilibrium conditions. All the kinetic case results fell between these two bounding cases.

Comparisons of Cases 1 through 4, as summarized in Table 3.2, clearly demonstrate the interaction of dissolving solids and aqueous species. Solids concentrations decrease and aqueous concentrations increase as dissolution rates ($k_2$ values) increase. Furthermore, these chemical composition changes caused by the solids dissolution is changing physical properties and rheology, (e.g., densities of solution and sledges and yield/shear stresses). For example, the model predicted that yield stresses are generally lower in Case 1 than in Case 2, which, in turn, are three to five times lower than Case 3 at 15 minutes. The model also predicted that the more solids dissolution, the greater the supernatant density. These changes in physical properties and rheology in turn affected the flow field, as shown in Figures 3.11, 3.15, and 3.19 for Cases 1, 2, and 3, respectively. These figures reveal that, among other aspects, the greater the solid dissolution, the smaller the maximum velocity.

Cases 1 through 5, with varying degrees of incorporation of chemical equilibrium reactions and kinetic reaction rates, demonstrate that the modified TEMPEST code can predict distributions of reactive solids and aqueous species by taking into account 1) fast equilibrium chemistry, 2) slow kinetic chemistry, and 3) some associated changes in physical properties and rheology, under the relatively simple decayed jet tank segment model conditions. These test results revealed that fast and slow chemical reactions affect physical properties and rheology, changing, for example, yield stress, viscosity, supernatant liquid density, and compositions of the solids, aqueous, and gaseous constituents. These changes, in turn, affect the flow movements and distributions of chemical constituents in the tank. Thus, although these cases are considerably simpler than actual physical and chemical processes in the Hanford waste tanks, these modeling exercises reveal that the interactions between solids dissolution/precipitation and physical transport processes are important enough to incorporate into tank waste dilution evaluations.

## 3.3 Detailed Dilution Injection Model Results and Evaluations

For the dilution injection model, we also ran five cases to further test the modified TEMPEST and evaluate the effects of solids dissolution/precipitation on physical properties and of rheology on distributions of velocity and constituents. In the analysis, Cases 1 and 3 incorporate physical mixing, chemical equilibrium, and kinetic reactions. As discussed in Section 3.2.2, Cases 1 and 2 have relatively realistic dissolution kinetic rates. Case 4 includes only physical mixing and equilibrium chemical reactions without kinetic reactions, and Case 5 incorporates only physical mixing without considering any chemical reactions.

### 3.3.1 Results of the Dilution Injection Model Runs

We ran Cases 1 through 3 for 15 minutes and Cases 4 and 5 for 100 seconds. Similar to the decayed jet tank segment cases, we simulated both the chemical equilibrium and kinetic

reactions for only once per 100 time steps for all four simulation cases. Since the simulation time steps were about 2 milliseconds for the dilution injection runs, chemistry was still simulated for approximately every 0.2 second.

Because there is a large density difference between the injected water and the sludge, the flow pattern (especially in the early stage) is for the diluent to turn and flow directly upward along the pipe to the surface, as shown in Figure 3.24 at the predicted time, 0.476 second. This figure shows the velocity near the bottom left to be relatively large, but the flow does not penetrate through the solid tank bottom. We will first present some of the predicted results for these four cases, followed by their evaluations.

For Case 1 (physical mixing and chemistry with the kinetic rate of $k_2 = 0.003/s$), Figure 3.25 show predicted time-varying volume fractions of reactive solids of $NaNO_3(s)$ at two locations (locations 1 and 4) in the study area over 15 minutes; Figure 3.25 also shows the corresponding values of $NaNO_2(s)$ at location 1. Location 1 is approximately 0.6 m from the tank center and 1.54 m above the tank bottom. Location 4 is 1.1 m from the center and 0.28 m above the tank bottom. Figure 3.26 presents predicted time-varying distributions of the nonreactive Solid 4 and $H_2/N_2$ gases at location 1 over 15 minutes for comparisons with reactive solids distributions. The predicted spatial distribution of the reactive $NaNO_3(s)$ is presented in Figure 3.27 at 15 minutes; the predicted velocity distribution at 15 minutes is shown in Figure 3.28. Case 2 results show a similar trend but with less solids dissolution.

For Case 3 (physical mixing and chemistry with the kinetic rate of $k_2 = 1 \times 10^{-6}$ /s), the temporal variation of the predicted $NaNO_3(s)$ concentrations (volume fraction) over 15 minutes is shown in Figure 3.29 with those of Cases 1 and 2, while Figure 3.30 depicts a calculated spatial distribution of $NaNO_3(s)$ at 15 minutes.

For Case 4 (physical mixing and equilibrium chemistry without kinetic reactions), the calculated temporal variation of $NaNO_3(s)$ volume fractions over one minute is shown in Figure 3.31, while its spatial variation at 100 seconds is shown in Figure 3.32.

Figure 3.33 presents the predicted spatial variation of $NaNO_3(s)$ volume fractions at 100 seconds for Case 5 (physical mixing only without chemical reactions).

### 3.3.2 Evaluations of the Dilution Injection Model Runs

Similar to the decayed jet tank segment model cases, the modified TEMPEST predicted distributions of two reactive solids [$NaNO_3(s)$ and $NaNO_2(s)$], two nonreactive solids, $H_2/N_2$ gas, $H_2O$, and five aqueous chemical species [i.e., $Na^+$, $NO_3^-$, $NO_2^-$, $NaNO_3(aq)$, and $NaNO_2(aq)$] in a tank by taking into account the chemical reactions and their impacts on physical properties and rheology. This is again shown by comparing temporal variations of predicted distributions of the 11 constituents at various locations over 15 minutes. In Case 1, predicted distributions of $NaNO_3(s)$ volume fractions over 15 minutes, for example, are reduced by about four to six times to approximately 0.042 and 0.031, respectively, as shown in Figure 3.25. Those of $NaNO_2(s)$are reduced by about six times to approximately 0.031, also shown in Figure 3.25. The lower

concentrations of $NaNO_2(s)$ were due to its predicted solubility limit being lower than that of $NaNO_3(s)$. These reductions are more than twice those of nonreactive constituents experienced during the same 15-minute period because of the continuous injection of water into the study tank, as shown in Figure 3.26. These differences are mostly due to the dissolution of the reactive $NaNO_3(s)$ and $NaNO_2(s)$. Note that Case 1 has a faster expected range of solids dissolution rates, while the Case 2 range is at the slower end of the expected range, as discussed in Section 3.2.2. The comparisons of these reactive and nonreactive constituents clearly demonstrated that the modified TEMPEST predicted chemical reactions in addition to the physical mixing in a predictable manner.

The kinetic effects on chemical concentrations were also clearly revealed by the modified TEMPEST code by comparing Figures 3.25 and 3.29, as well as Figures 3.27 and 3.30 of Cases 1 through 3. These figures show that concentrations of $NaNO_3(s)$ for Case 1 are smaller than the concentrations for Case 3 with very small kinetic rate of $1 \times 10^{-6}$ per second due to the much greater solids dissolution occurring for Case 1. The results for Case 2 fell between those of Cases 1 and 3, as expected. The reduction in Cases 3 and 5 (physical mixing only case) is basically due to the physical mixing and flushing of the original solids. The differences among Cases 1 through 3 become greater with time as more dissolution occurs (see Figure 3.29). The dissolution of the reactive solids would keep changing aqueous species concentrations, indicating that the greater the dissolution rates ($k_2$ values), the smaller the solids concentrations and the larger the aqueous concentrations become. This is clearly shown in Table 3.3, which presents predicted representative chemical concentrations at 15 minutes for Cases 1 through 3. These concentrations were approximately 1.21 m away from the tank center and 1.13 m above the tank bottom.

**Table 3.3.** Predicted Chemical Concentrations ($kg/m^3$) at 15 Minutes for Cases 1 through 3 of the Dilution Injection Model

| Chemical Species | Initial Concentrations ($kg/m^3$) | Case 1 Fastest Kinetics Concentrations ($kg/m^3$) | Case 2 Slower Kinetics Concentrations ($kg/m^3$) | Case 3 Very Slow Kinetics Concentrations ($kg/m^3$) |
|---|---|---|---|---|
| $NaNO_3(s)$ | 430 | 94 | 152 | 226 |
| $NaNO_2(s)$ | 398 | 67 | 129 | 209 |
| $Na^+$ | 117 | 139 | 112 | 73 |
| $NO_3^-$ | 137 | 166 | 129 | 79 |
| $NO_2^-$ | 133 | 155 | 128 | 87 |
| $NaNO_3(aq)$ | 38 | 33 | 22 | 10 |
| $NaNO_2(aq)$ | 87 | 71 | 46 | 20 |

These tests further confirm that the TEMPEST is reproducing the expected trend of the chemical concentrations with solid dissolution/precipitation reactions. Note that Case 1 has a faster end of the expected solids dissolution rate change, as discussed in Section 3.2.1. However, unlike the corresponding decayed jet tank segment model case, they are not reaching their equilibrium values at the end of 15 minutes. This is because the flow is continuously poured into and out from the simulation area, thus the solids may or may not have a contact with the same supernate for 15 minutes to reach their equilibrium values. The potential for not reaching equilibrium conditions must be taken into consideration when actual tank dilution is implemented.

Case 4 (physical mixing and equilibrium chemistry) is a limiting case where all reactions, including dissolution/precipitation, would occur instantaneously. In our actual modeling run, the instantaneous reactions means that all chemical reactions will reach their equilibrium conditions within approximately 0.2 seconds, while the equilibrium conditions themselves are keep changing due to physical mixing. Although this is not realistic, the TEMPEST results indicated that predicted reactive solids concentrations are smaller than those with kinetic and no chemistry cases (Cases 1, 2, 3, and 5), as expected (see Figures 3.29 and 3.31). As discussed above, it is possible that equilibrium conditions may not be achieved for these solids even over a long time.

In Case 5 (physical mixing only with neither fast-equilibrium nor slow-kinetic reactions occurring), $NaNO_{3(s)}$ and $NaNO_{2(s)}$ behaved as chemically nonreactive. Thus, TEMPEST indicated that this case also constitutes another bounding case for the dilution injection model. Because $NaNO_{3(s)}$ and $NaNO_{2(s)}$ in the other four cases are dissolving, Case 5, with only physical mixing, has the highest concentrations of $NaNO_3$(s) and $NaNO_2$(s), while Case 4 has the lowest concentrations, as revealed through the comparison of predicted $NaNO_3$(s) concentrations of the bounding Cases 4 and 5 shown in Figures 3.32 and 3.33. The maximum volume fraction for the physical-mixing-only case has been diluted from the initial condition of 0.191 to about 0.185 because of diluent transport effects over 100 seconds and to 0.175 in Case 4, which is subject to diluent transport and instantaneous solids dissolution.

The pure water jet rises rather rapidly along the pipe because of its buoyancy and leaves a large portion of the study area originally undisturbed (see Figure 3.24). This is clearly shown in spatial distributions of $NaNO_3$(s) and $NaNO_2$(s) not only at 1 minute but even after 15 minutes (see Figures 3.27 and 3.30). The results of Cases 1 and 2 indicate that the reduction of solids ($NaNO_3$(s) and $NaNO_2$(s)) occurs farther away from the pipe as the diluent induces chemical dissolution. Although this process is very slow and not dramatic, it progresses as reactive solids are dissolved, reducing the sludge shear resistance and allowing more flow to penetrate into the interior. For example, the lower solids concentrations resulting from the solids dissolution decrease more yield stress than the cases without dissolution. The yield stresses in the lower exterior far-field show consistently lower values in cases with the chemistry simulations compared with Case 5 without chemical reactions. As in the cases of decayed jet tank segment model, the supernatant and sludge densities calculated by TEMPEST were also affected by the chemical reactions occurring during the simulation period. Although it is rather difficult to discern the effects of chemical composition changes caused by solid dissolution on the physical property and rheology changes, they are influencing the predicted velocity distributions, as shown in Figure 3.28 for Case 1.

The modified TEMPEST code simulated flow-field conditions resembling an immediate vicinity of the jet injection point in a waste tank with varying degrees of incorporation of chemical reactions. The model results suggest that the chemical reactions can affect compositions of the solids, aqueous, and gaseous constituents, and physical properties and rheology (e.g., yield stress, viscosity, and supernate density). They also suggest a possibility of not reaching equilibrium conditions even with a large amount of time, because of changing tank conditions. This possibility must be carefully examined when the actual tank waste dilution is implemented.

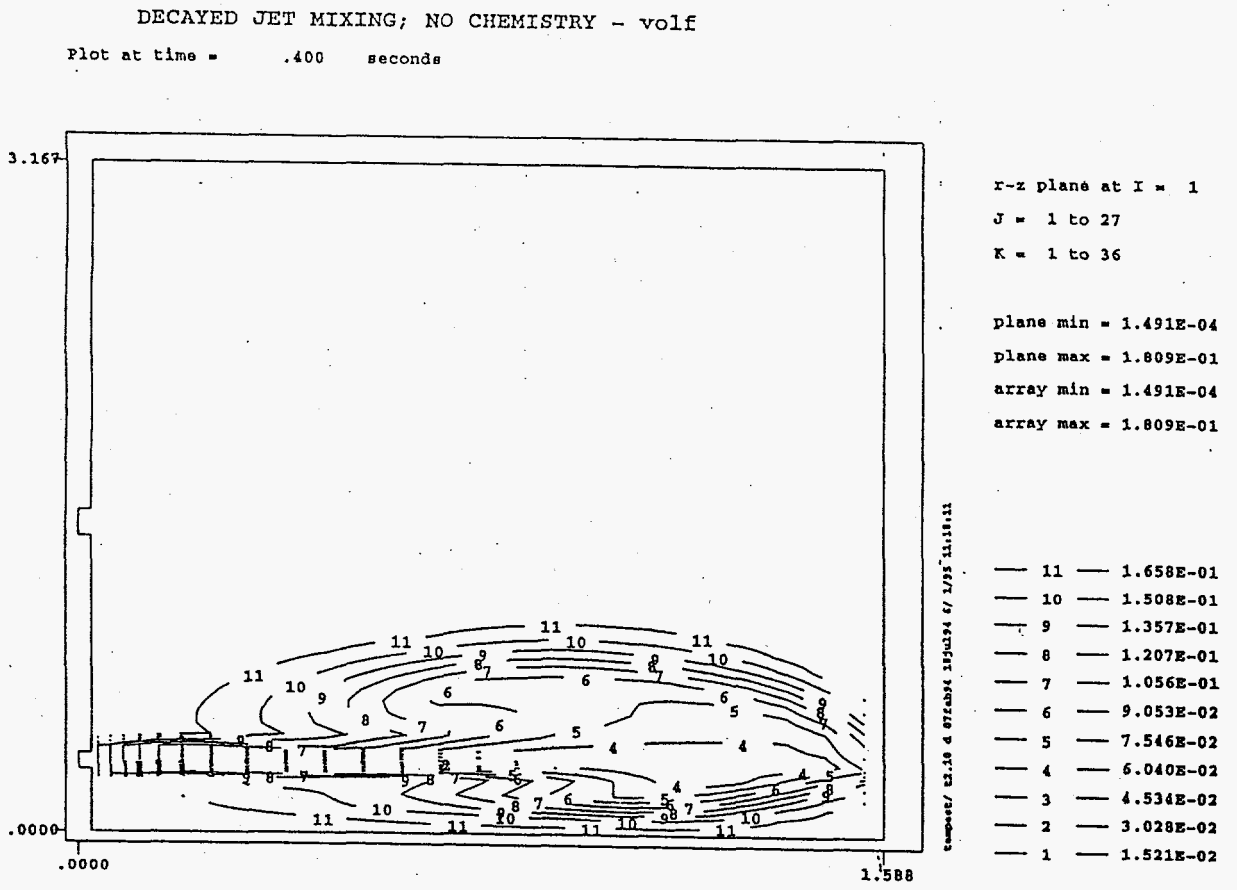


**Figure 3.4.** $NaNO_3$(s) at 0.4 Second for Case 5

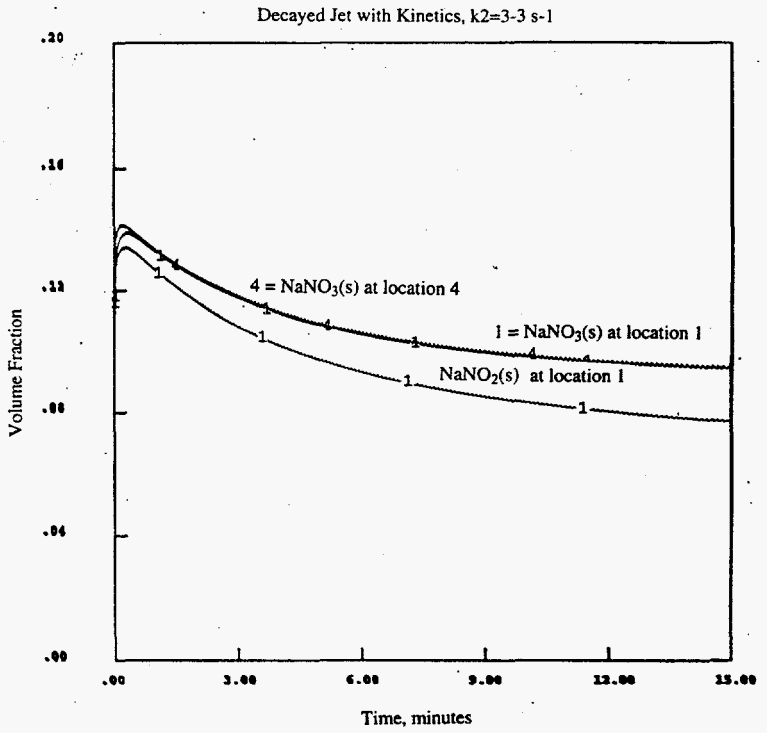


**Figure 3.5.** $NaNO_3(s)$ and $NaNO_2(s)$ for Case 1

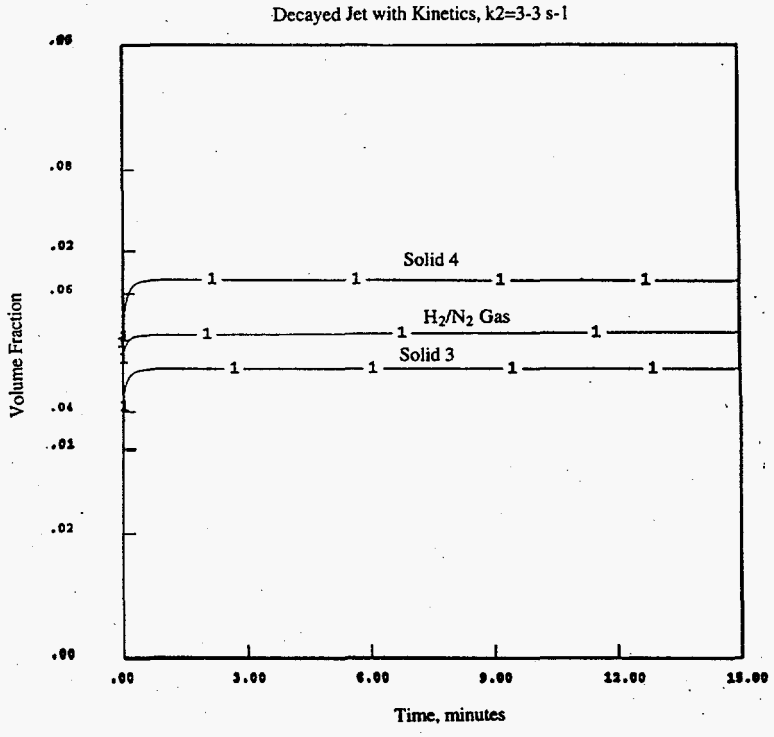


**Figure 3.6.** Nonreactive Solids 3 and 4, $H_2/N_2$ Gas at Location 1 for Case 1

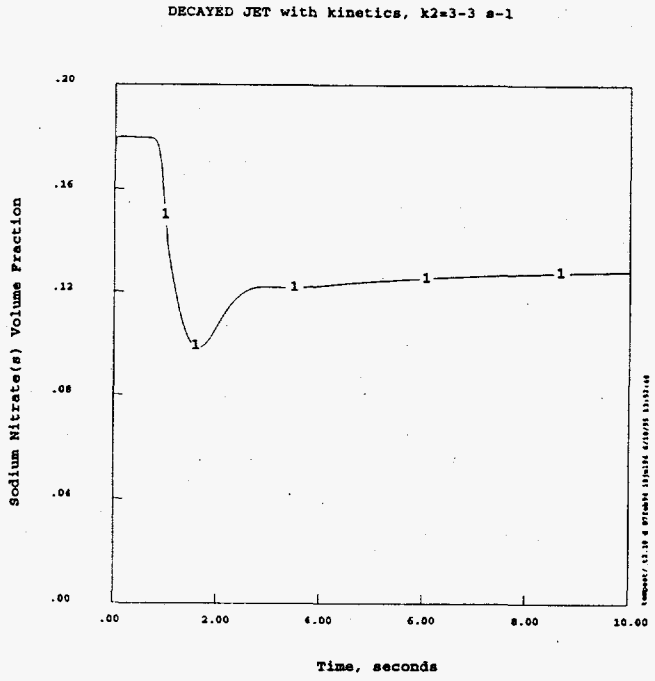


**Figure 3.7.** $NaNO_3$(s) Over 10 Seconds at Location 1 for Case 1

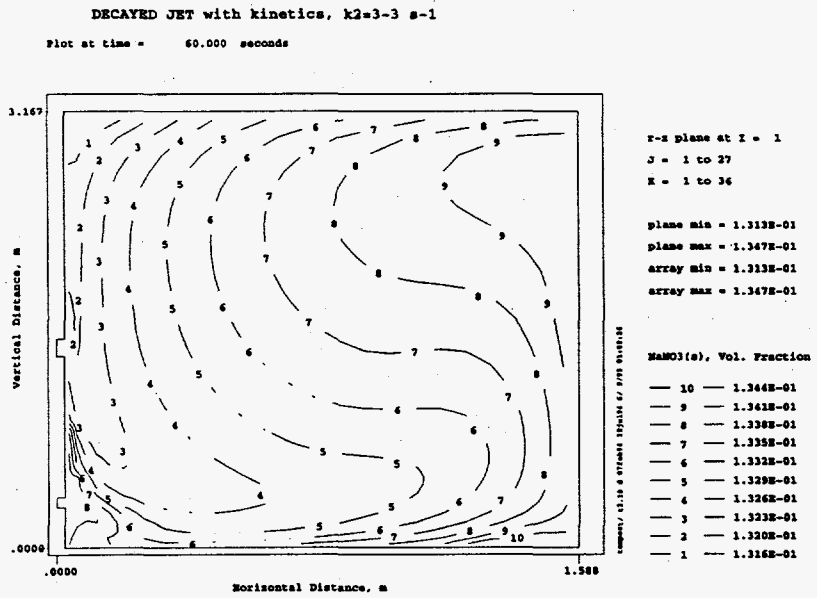


**Figure 3.8.** $NaNO_3$(s) at One Minute for Case 1

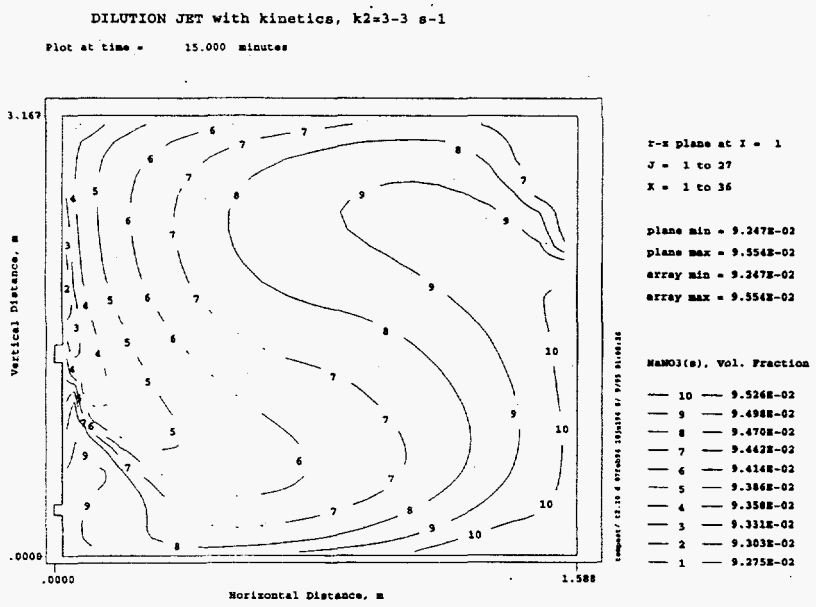


**Figure 3.9**. $NaNO_3$(s) at 15 Minutes for Case 1

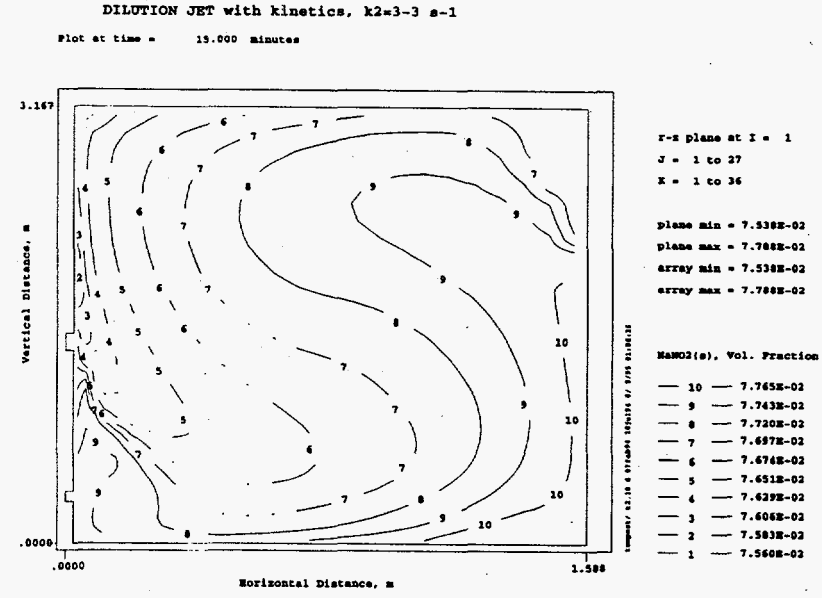


**Figure 3.10.** $NaNO_2$(s) at 15 Minutes for Case 1

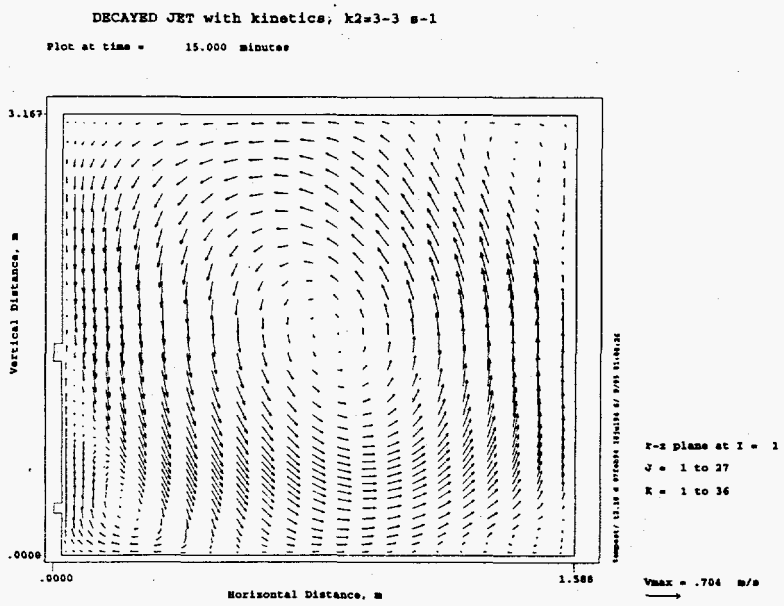


**Figure 3.11.** Velocity Distribution at 15 Minutes for Case 1

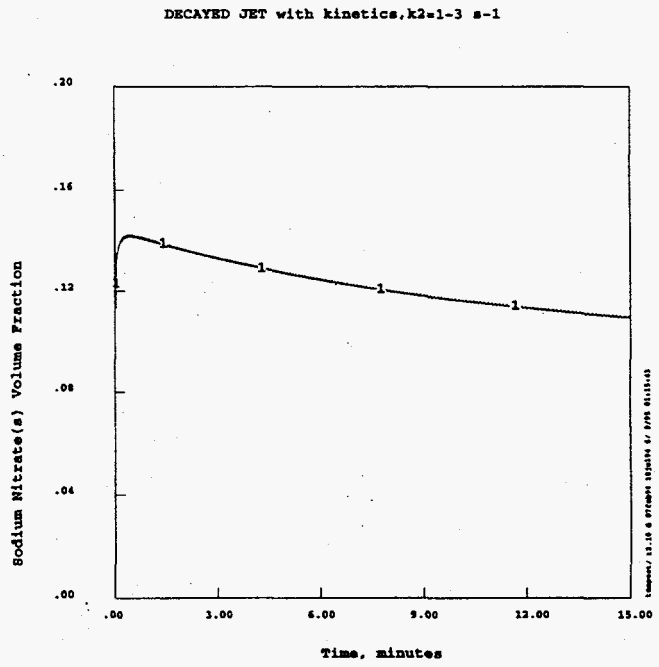


**Figure 3.12.** $NaNO_3(s)$ Over 15 Minutes at Location 1 for Case 2

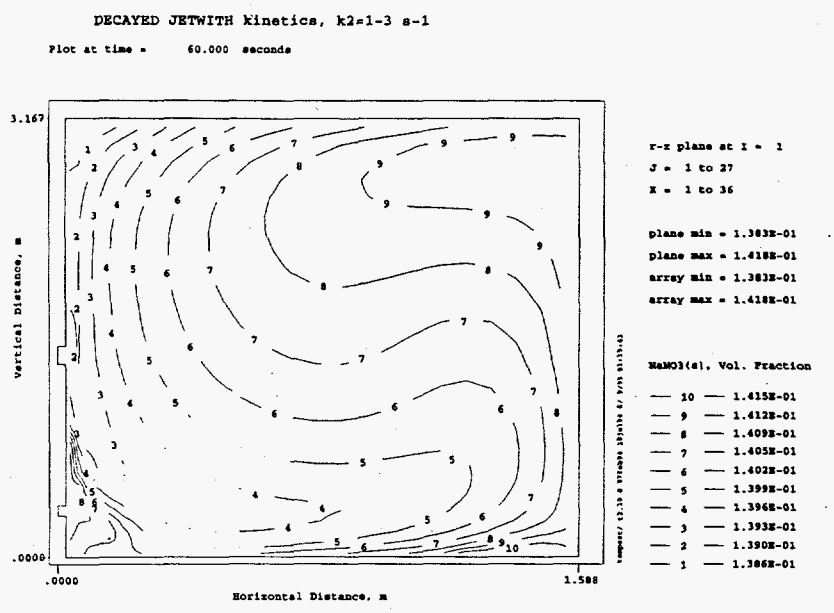


**Figure 3.13.** $NaNO_3$(s) at One Minute for Case 2

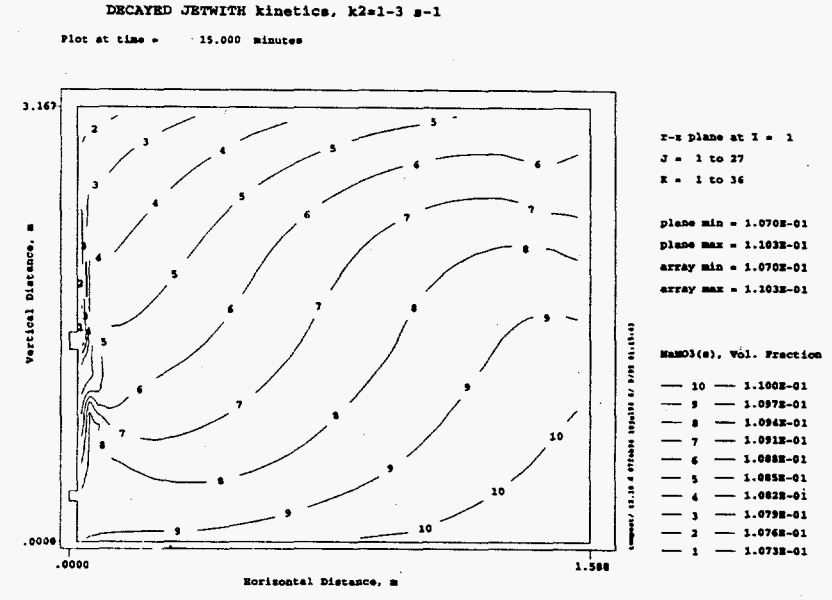


**Figure 3.14.** $NaNO_3$(s) at 15 Minutes for Case 2

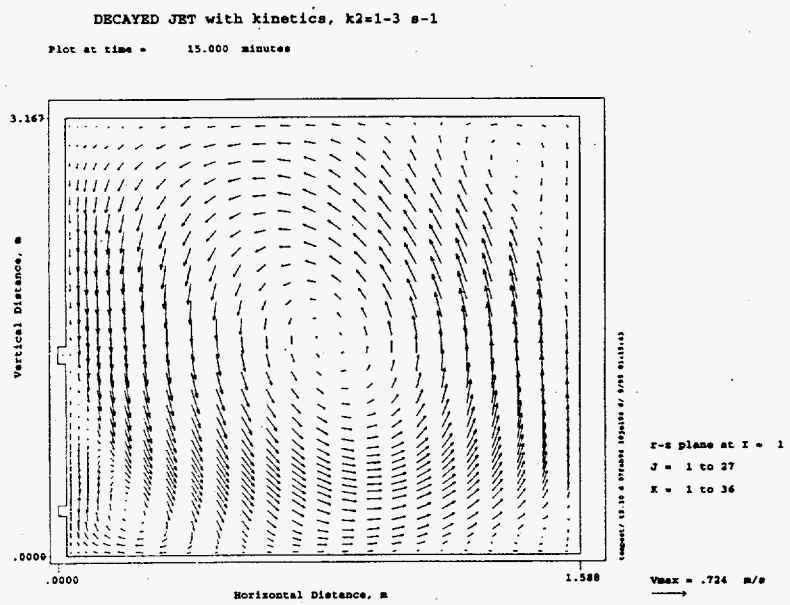


**Figure 3.15**. Velocity Distribution at 15 Minutes for Case 2

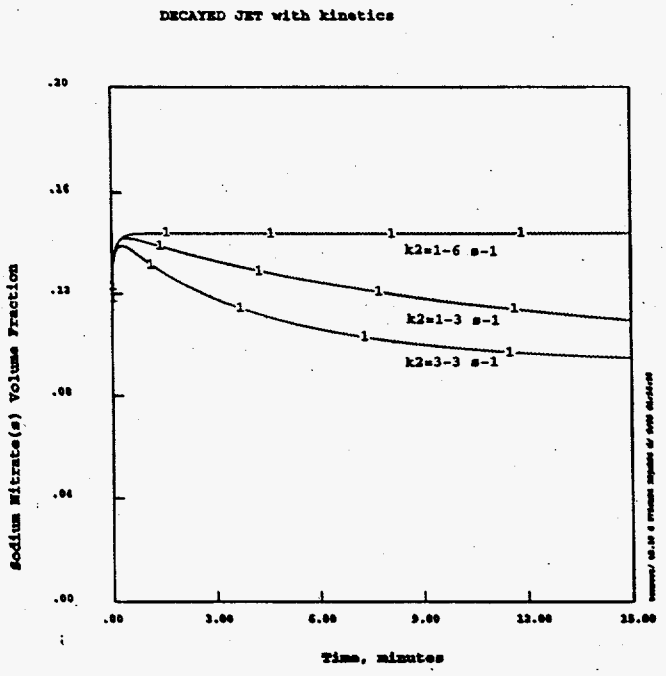


**Figure 3.16**. $NaNO_3$(s) Over 15 Minutes at Location 1 for Cases 1–3

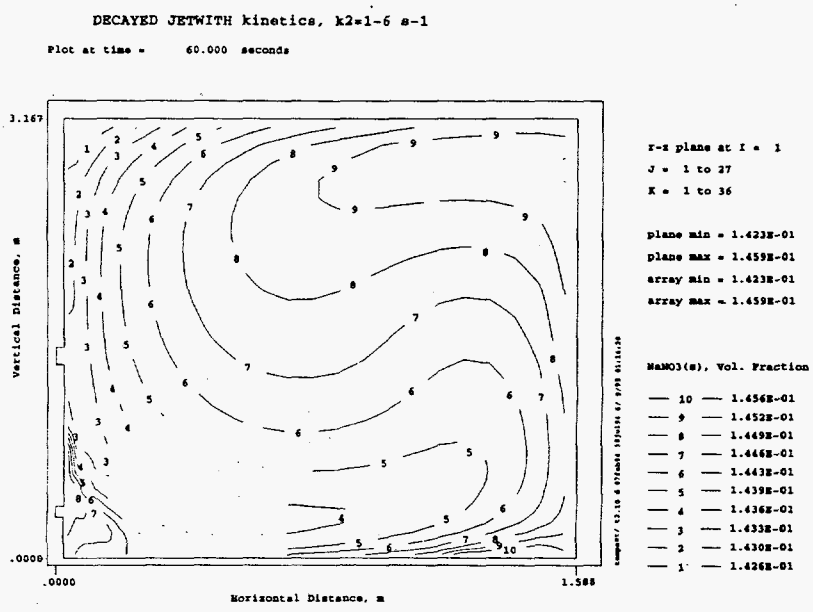


**Figure 3.17**. $NaNO_3$(s) at One Minute for Case 3

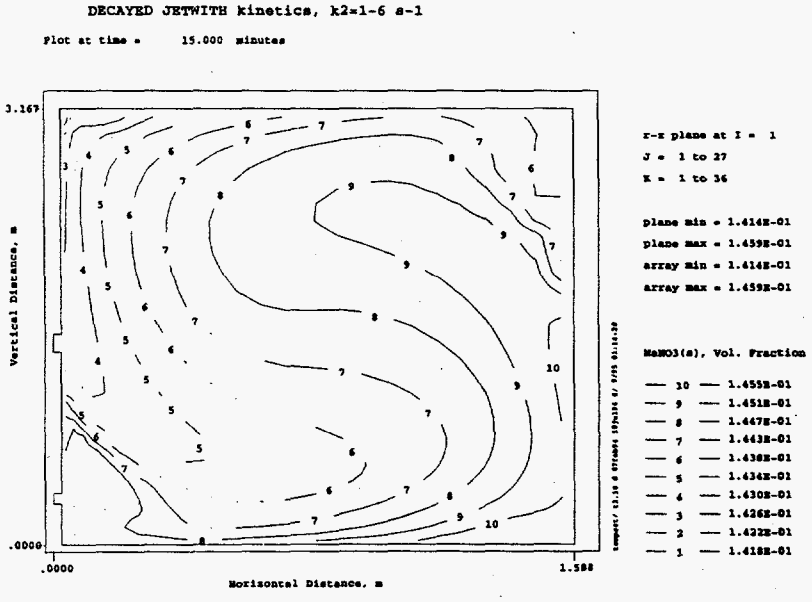


**Figure 3.18**. $NaNO_3$(s) at 15 Minutes for Case 3

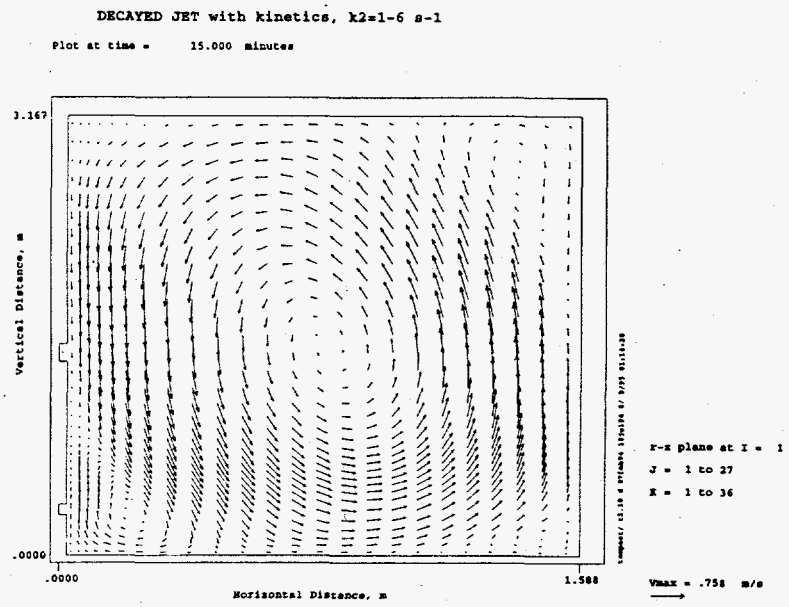


**Figure 3.19**. Velocity Distribution at 15 Minutes for Case 3

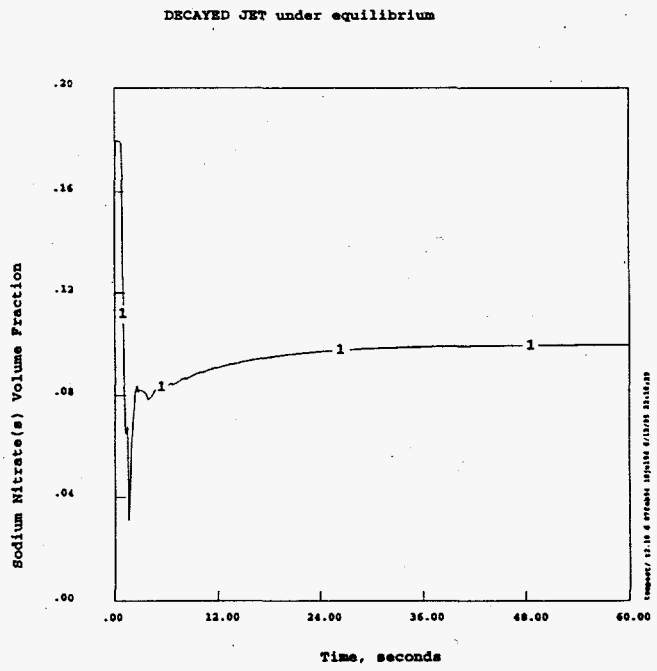


**Figure 3.20**. $NaNO_3(s)$ Over One Minute at Location 1 for Case 4

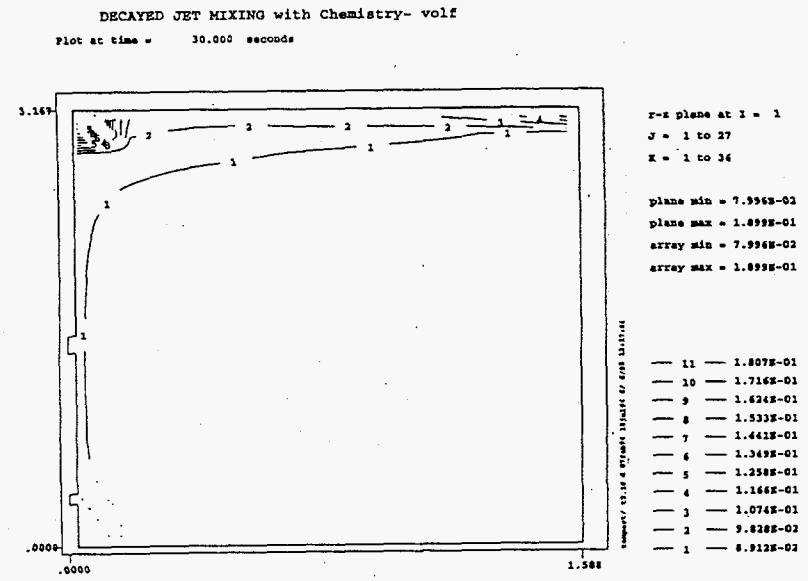


**Figure 3.21.** $NaNO_3$(s) at 30 Seconds for Case 4

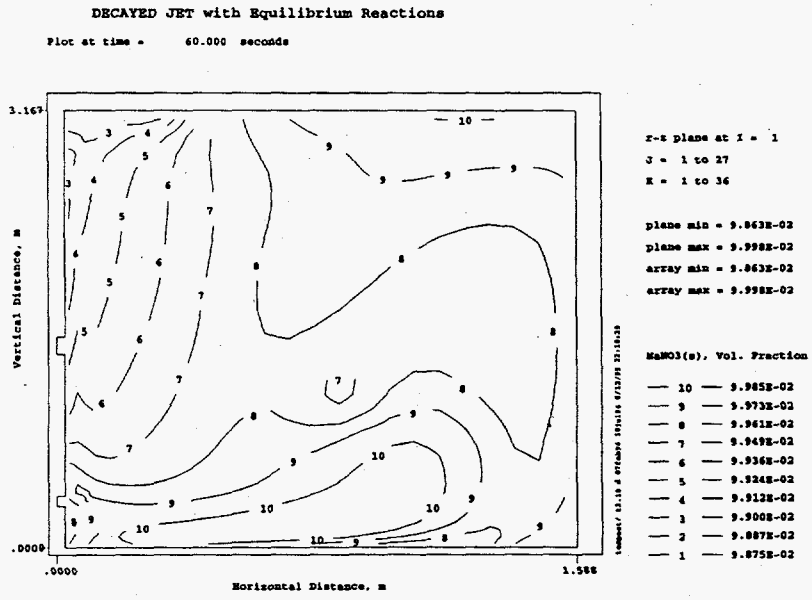


**Figure 3.22.** $NaNO_3$(s) at One Minute for Case 4

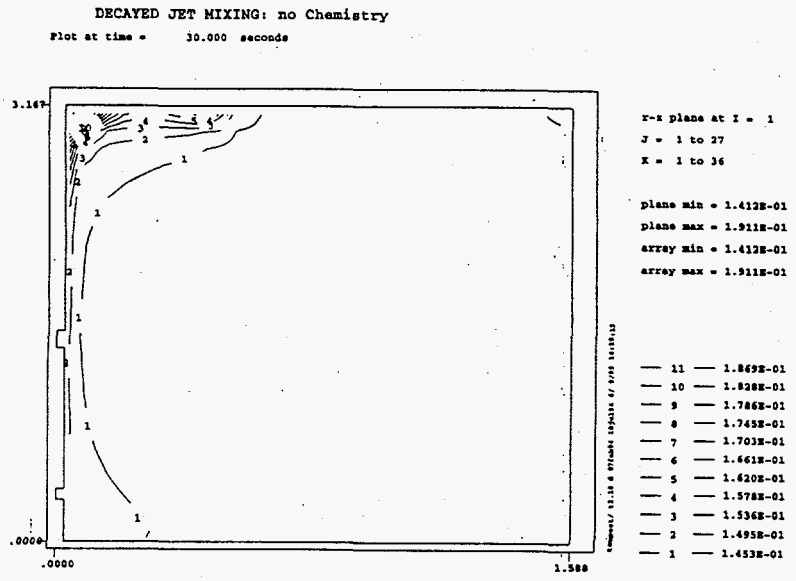


**Figure 3.23.** $NaNO_3$(s) at 30 Seconds for Case 5

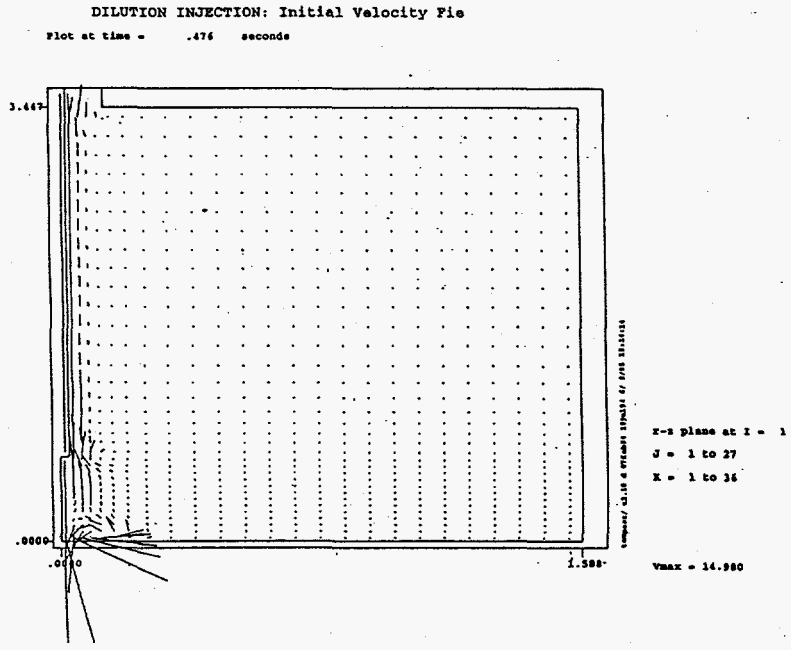


**Figure 3.24.** Velocity Distribution at 0.476 Second for Case 4

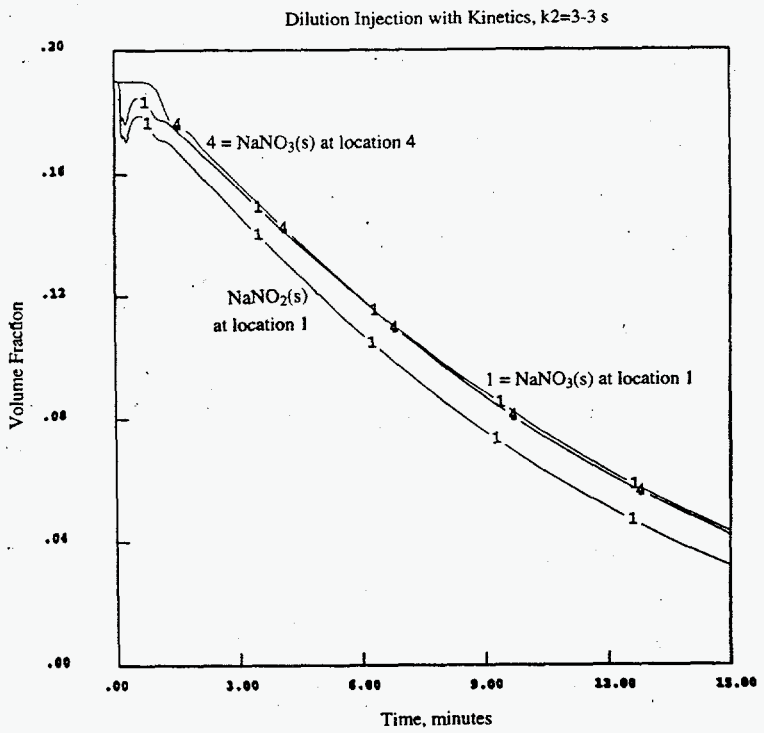


**Figure 3.25**. $NaNO_3(s)$ and $NaNO_2(s)$ Over 15 Minutes for Case 1

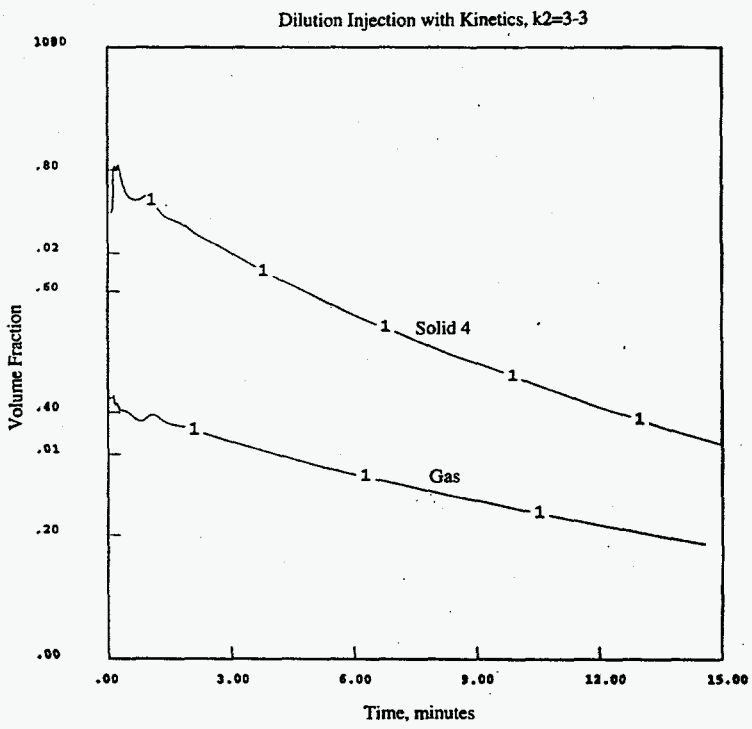


**Figure 3.26**. Nonreactive Solid 4 and $H_2/N_2$ Gas Over 15 Minutes at Location 1 for Case 1

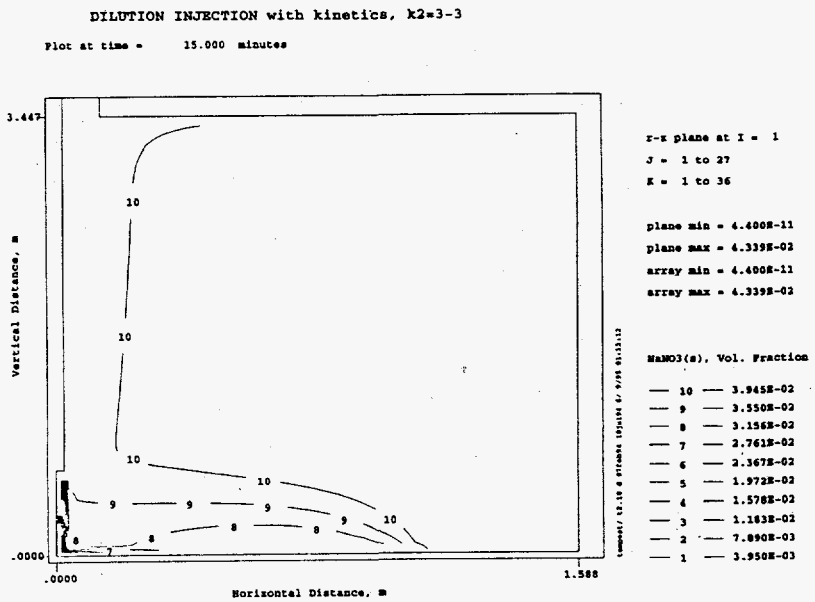


**Figure 3.27.** $NaNO_3(s)$ at 15 Minutes for Case 1

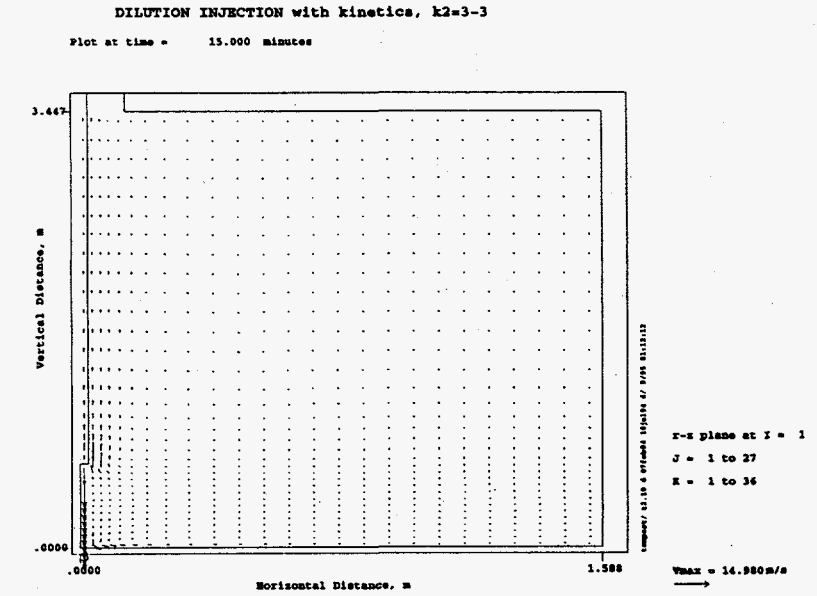


**Figure 3.28.** Velocity Distribution at 15 Minutes for Case 1

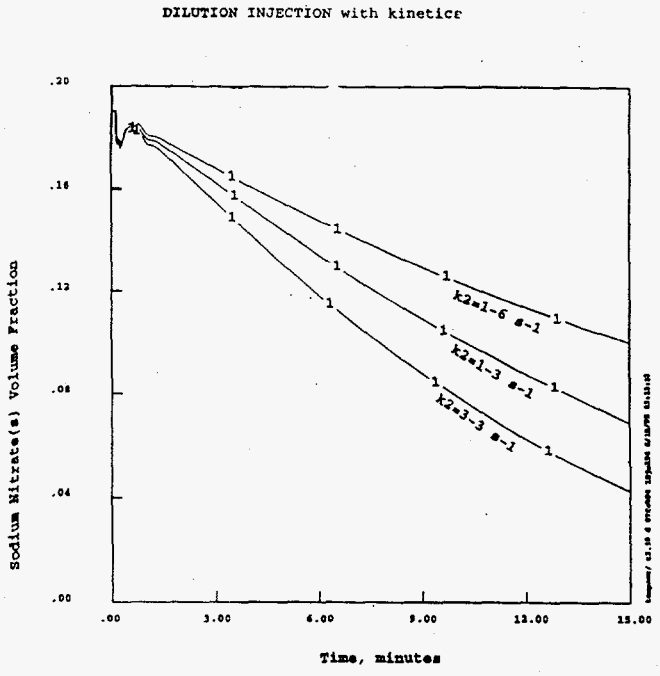


**Figure 3.29.** $NaNO_3(s)$ at 15 Minutes at Location 1 for Cases 1–3

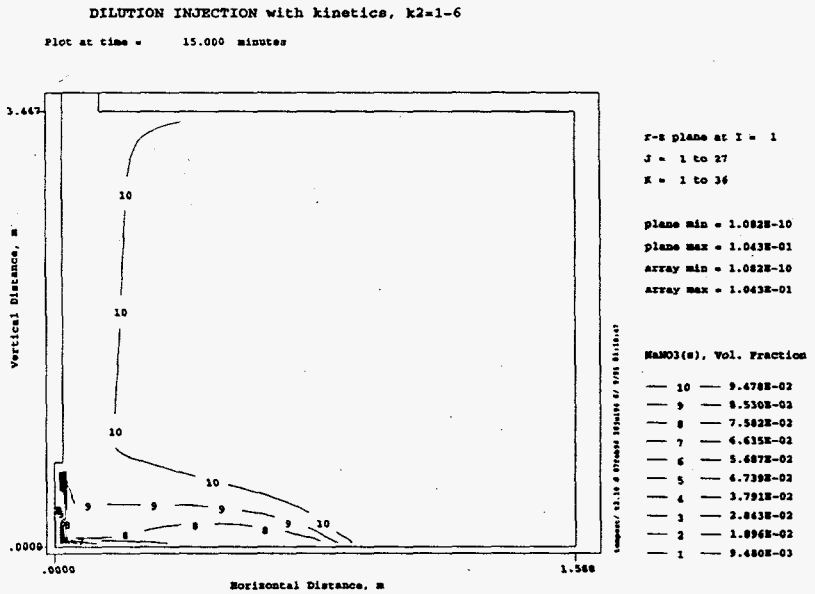


**Figure 3.30.** $NaNO_3(s)$ at 15 Minutes for Case 3

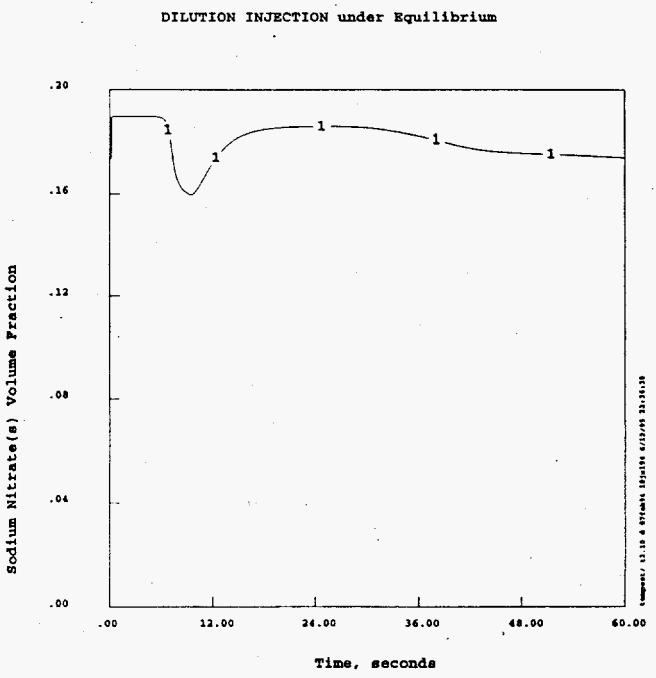


**Figure 3.31.** $NaNO_3(s)$ Over One Minute at Location 1 for Case 4

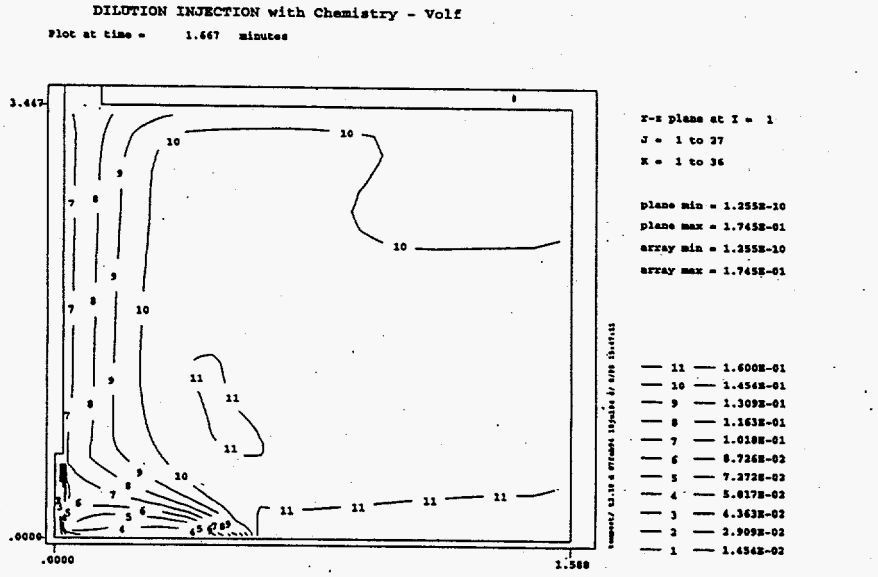


**Figure 3.32.** $NaNO_3(s)$ at 100 Seconds for Case 4

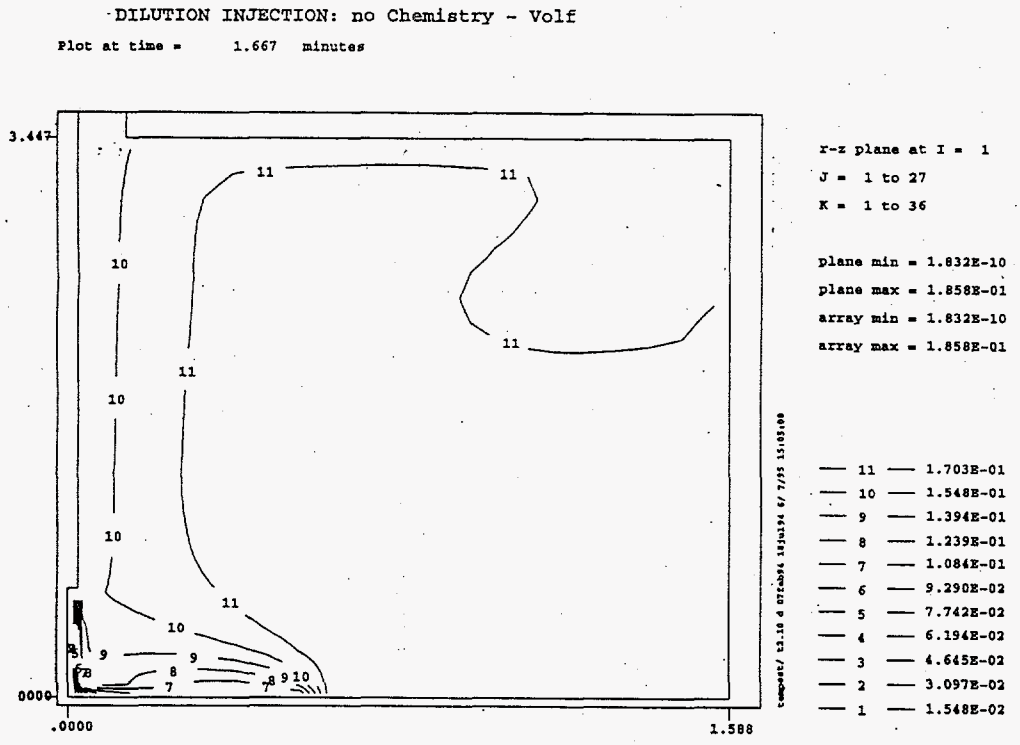


**Figure 3.33.** $NaNO_3$(s) at 100 Seconds for Case 5

# 4.0 Conclusions and Recommendations

The solids dissolution and precipitation affect the physical behavior of tank wastes, including gas retention in the sludge layer, solids resuspension and settling, and convective flow and physical species motions. To improve the reliability of tank waste simulation, we modified the TEMPEST code to include equilibrium and kinetic modeling capabilities.

The modified TEMPEST was then tested for the decayed jet tank segment and the dilution injection test cases. These cases covered varying degrees of incorporation of chemical equilibrium and kinetic reaction effects. The model results demonstrate that the modified TEMPEST can predict distributions of reactive solids and aqueous species by taking into account fast equilibrium chemistry, slow kinetic chemistry, and some associated changes on physical properties and rheology, under relatively simple test conditions resembling the potential conditions of jet injection into a waste tank. These model results also indicate that both fast and slow chemical reactions such as changing yield stress, viscosity and supernatant density, and compositions of the solids, aqueous, and gaseous constituents, can affect physical properties and rheology. These changes, in turn, affect the movements and distributions of flow and chemical constituents in the tank. Although these test conditions are considerably simpler than actual physical and chemical conditions occurring in the Hanford waste tanks, these modeling exercises reveal that solid dissolution and precipitation are potentially important processes that should be incorporated into tank waste evaluations under natural and engineered conditions affecting chemistry.

The dilution injection test cases also revealed the possibility of not reaching equilibrium conditions even with a large amount of time because of changing chemical and physical tank conditions. This possibility must be carefully examined if actual tank waste dilution is further considered.

The modified code has the following limitations:

- Restricted technical feasibility due to limited knowledge of
  - tank waste characterization
  - chemistry in the tanks
  - complex organic chemistry
  - interaction of organic and inorganic chemistry
  - dissolution/precipitation kinetic rates
  - gas generation and movements
  - physical behavior of solids (e.g., yield strength)
  - rheological correlations applicable to Hanford tank waste conditions
- Cost/time limitations due to
  - slow computational speed, especially for the chemical modeling
  - requirement of very small computational time steps during a period of fast waste movement.

However, many of these limitations can be overcome as we incorporate new knowledge and approaches. And, even with these limitations, the modified code can address many important interactions between the chemical and physical transport in the tanks.

When TEMPEST is fully integrated with chemical reactions and associated rheology improvements, it is expected to be able to predict the following:

- Dissolution/precipitation such that evolving chemical concentrations are available for estimating physical properties and rheology
- Adsorption/desorption reactions (if applicable) affecting chemical compositions
- The pH and other chemical variables for improved predictions of effective viscosity and other rheology
- Behavior of chemically reactive gas and solid fractions affecting gas retention.

To achieve these goals, we recommend the following:

- Test the modified TEMPEST for additional, more complex chemical conditions, similar to actual Hanford tank conditions, including potential pH changes.
- Incorporate the thermodynamic database being developed under the Pretreatment Program.
- Incorporate reactive gas (e.g., $NH_3$ gas) modeling capabilities.
- Improve the equilibrium modeling computation efficiency.
- Improve overall computational efficiency by adapting parallel processing capabilities.
- Relate particle size distributions to solids precipitation and incorporate into TEMPEST.
- Incorporate pH-rheology relationships.
- Develop and implement chemical reactions and a sludge yield strength relationship.

The improved TEMPEST will then be able to address chemically and physically interacting complex processes more broadly and reliably , including dilution of tank wastes, mixing of various tank wastes, flammable gas behavior, and waste treatment processes.

# 5.0 References


Allemann, R. T., Z. I. Antoniak, W. D. Chvala, L. E. Efferding, J. D. Fadeff, J. R. Friley, W. B. Gregory, J. D. Hudson, J. J. Irwin, N. W. Kirch, T. E. Michener, F. E. Panisko, C. W. Stewart, and B. M. Wise. 1994. *Mitigation of Tank 241-SY-101 by Pump Mixing: Results of Testing Phases A and B.* PNL-9423, Pacific Northwest Laboratory, Richland, Washington.

Antoniak, Z. I. 1994. *Historical Trends in Tank 241 SY-103 Waste Temperatures.* PNL-10058, Pacific Northwest Laboratory, Richland, Washington.

Babad, I., H., J. L. Deichman, B. M. Johnson, D. K. Lemon, and D. M. Strachan. 1992. *Mitigation/Remediation Concepts for Hanford Site Flammable Gas Generating Waste Tanks.* WHC-EP-0516, Westinghouse Hanford Company, Richland, Washington.

Felmy, A. R. 1990. *GMIN: A Computerized Chemical Equilibrium Model Using a Constrained Minimization of the Gibbs Free Energy.* PNL-7281, Pacific Northwest Laboratory, Richland, Washington.

Gauglitz, P. A., S. D. Rassat, M. R. Powell, R. R. Shah, and L. A. Mahoney. 1995. *Gas Bubble Retention and Its Effects on Waste Properties: Retention Mechanisms, Viscosity, and Tensile and Shear Strengths.* PNL-10740, Pacific Northwest Laboratory, Richland, Washington.

Harvie, C. E., J. P. Greenberg, and J. H. Weare. 1987. "A Chemical Equilibrium Algorithm for Highly Non-Ideal Multiphase Systems: Free Energy Minimization." *Geochemica et Cosmochimica Acta*, Vol. 51, pp. 1045-1057.

Hudson, J. D., G. S. Barney, P. R. Bredt, A. R. Felmy, D. L. Herting, A. P. Larrick, D. A. Reynolds, C. W. Stewart, J. M. Tingey, and D. S. Trent. 1995. *An Assessment of the Dilution Required to Mitigate Hanford Tank 241-SY-101.* PNL-10417, Pacific Northwest Laboratory, Richland, Washington.

Mahoney, L. A., and D. S. Trent. 1995. *Correlation Models for Waste Tank Sludges and Slurries.* PNL-10695, Pacific Northwest Laboratory, Richland, Washington.

Pederson L. R., and D. M. Strachan. 1993. *Status and Integration of the Gas Generation Studies Performed for the Hydrogen Safety Program - FY 1992 Annual Report.* PNL-8523, Pacific Northwest Laboratory, Richland, Washington.

Rassat, S. D., and P. A. Gauglitz. 1995. *Bubble Retention in Synthetic Sludge: Testing of Alternative Gas Retention Apparatus.* PNL-10661, Pacific Northwest Laboratory, Richland, Washington.

Reynolds, D. A., and D. L. Herting. 1984. *Solubilities of Sodium Nitrate, Sodium Nitrite, and Sodium Aluminate in Simulated Nuclear Waste.* RHO-RE-ST-14P, Rockwell International, Richland, Washington.

Rieck, C. A. 1993. *Conceptual Design Report, Initial Tank Retrieval Systems, Project W-211.* WHC-SD-W211-CDR-001 Rev.0, Westinghouse Hanford Company, Richland, Washington.

Rodi, W. 1984. *Turbulence Models and Their Application in Hydraulics - a State of the Art Review.* Institut fur Hydromechanik, University of Karlsruhe, Germany.

Snoeyink, V. L., and D. Jenkins. 1980. *Water Chemistry.* John Wiley and Sons, New York.

Steefel, C. L., and A. C. Lasaga. 1994. "A Coupled Model for Transport of Multiple Chemical Species and Kinetic Precipitation/Dissolution Reactions with Application to Reactive Flow in Single Phase Hydrothermal Systems." *American Journal Of Science*, Vol. 294, pp. 529-592.

Steefel, C. L., And P. C. Lichtner. 1994. "Diffusion and Reaction in Rock Matrix bordering a Hyperalkaline Fluid-Filled Fracture." *Geochemica et Cosmochimica Acta*, 58(17): 3595-3612.

Stewart, C. W., L. A. Shienbein, J. D. Hudson, E. J. Eschbach, and D. L. Lessor. 1994. *Assessment of Alternative Mitigation Concepts for Hanford Flammable Gas Tanks.* PNL-10105, Pacific Northwest Laboratory, Richland, Washington.

Sawyer, C. N., P. L. McCarty, and G. F. Parkin. 1994. *Chemistry for Environmental Engineering.* McGraw-Hill Inc., New York.

Trent, D. S., and L. L. Eyler. 1988. *Numerical Methods and Input Instructions: TEMPEST -- A Three-Dimensional Time-Dependent Computer Program for Hydrothermal Analysis.* PNL-4348 Vol 1, Rev. 2, Pacific Northwest Laboratory, Richland, Washington.

Trent, D.S., and L.L. Eyler. 1994. *TEMPEST: A Computer Program for Three-Dimensional Time Dependent Computational Fluid Dynamics.* PNL-8857 Vol. 1, Version T, Mod 2, Pacific Northwest Laboratory, Richland, Washington.

Tank Waste Science Panel. 1991. *Chemical and Physical Processes in Tank 241-SY-101: A Preliminary Report.* PNL-7595, Pacific Northwest Laboratory, Richland, Washington.

Yeh, G. T., and V. S. Tripathi. 1989. "A Critical Evaluation of Recent Developments in Hydrogeochemical Transport Models of Reactive Multichemical Components." *Water Resources Research,* 25(1): 93-108.

# Distribution

No. of
Copies

OFFSITE

2 DOE Office of Scientific and Technical Information

N. W. Bibler
Westinghouse Savannah River Co.
Building 773A, Room B132
Box 616
Aiken, SC 29802

2 Department of Civil and Environmental Engineering
Washington State University
Pullman, WA 99164
Attn: M. Hanaif Chaudhry
R. Y Itani

J. A. Cochran, Dean
Washington State University, Tri-Cities
Richland, WA 99352

D. Cool, Chief
Radiation Protection and Health Effects Branch
Office of Research
U.S. Nuclear Regulatory Commisssion
Washington, D.C. 20555

Charles W. Forsberg
Oak Ridge National Laboratory
P.O. Box 2008, MS-6495
Oak Ridge, TN 37831-6495

M. Goldman
Laboratory for Energy-Related Health Research
University of California at Davis
Davis, CA 95616

No. of
Copies

E. P. Horwitz
Chemistry Department
Argonne National Laboratory
9700 Cass Avenue
Argonne, IL. 60439-4831

B. Hudson
PO Box 271
Lindsborg, KA 67456

K. Kim
H. Krumb School of Mines
Columbia University
809 Seely W. Mudd
New York, NY 10027

Thomas S. Kress
Oak Ridge National Laboratory
P.O. Box 2009
MS-8088, Bldg 9108
Oak Ridge, TN 37831-8088

R. B. Krone
Department of Civil and Environmental Engineering
University of California at Davis
Davis, CA 95616-5294

S. C. T. Lien, Director, EM-54
Office of Research and Development
Office of Technology Development
Office of Environmental Management
U.S. Department of Energy
Washington, D.C. 20585

No of
Copies

5 Los Alamos National Laboratory
P.O. Box 1663
Los Alamos, NM 87545
Attn: L. H. Sullivan, K557
J. R. White, K575
R. A. Tennant, J565
W. L. Kubic, K575
K. Pasamehmetoglu, K575

J. F. Paul
Environmental Research Laboratory
U.S. Environmental Protection Agency
Naragansett, RI 02882

D. Robey
Environmental Laboratory
Waterways Experimental Station
U.S. Army Corps of Engineers
Vicksburg, MS 39180

W. R. Rossen
Dept. of Petroleum/Geosystems Engineering
University of Texas at Austin
Austin, TX 78712-3246

A. Schneider
Massachussetts Institute of Technology
Department of Nuclear Engineering
Room 24-1098
77 Massachussetts Avenue
Cambridge, MA 02139

G. L. Schnoor
Center for Global and Regional Environmental Research
Department of Civil and Environmental Engineering
University of Iowa
Iowa City, IA 52242

No of
Copies

Scott E. Slezak
Sandia National Laboratory
Division 6415/MS 0741
P.O. Box 5800
Albuquerque, NM 87185

J. E. Till, President
Radiological Assessment Corp.
Rt. 2, Box 122
Neeses, SC 29107

J. Tseng
U.S. Department of Energy
Trevion II Building, EM-35
Washington, D.C. 20585-0002

2 U.S. Environmental Protection Agency
Office of Radiation Programs
401 M Street SW
Washington, D.C. 20460
Attn: R. Dyer
K. W. Yeh

**Onsite**

9 DOE Richland Operations Office

| | |
|---|---|
| D. H. Alexander | S7-51 |
| S. T. Burnum | S7-53 |
| R. F. Christensen | S7-54 |
| R. E. Gerton | S7-54 |
| J. M. Gray | S7-54 |
| C. A. Groendyke | S7-54 |
| M. F. Jarvis | S7-54 |
| Y. G. Noorani | R3-77 |
| G. W. Rosenwald | S7-54 |

No of Copies

36 Westinghouse Hanford Company

| | |
|---|---|
| H. Babad | S7-30 |
| G. S. Barney | T5-12 |
| W. B. Barton | H5-21 |
| K. G. Carothers | R1-51 |
| R. J. Cash | S7-15 |
| G. Galbraith | H2-52 |
| C. E. Hanson | H5-09 |
| J. P. Harris | S6-12 |
| D. L. Herting | T6-09 |
| J. O. Honeyman | S7-81 |
| J. D. Hopkins | R2-11 |
| J. Jewett | T6-09 |
| G. D. Johnson (5) | S7-15 |
| J. W. Lentsch (5) | S7-15 |
| J. M. Light | B4-08 |
| E. J. Lipke | S7-14 |
| N. G. McDuffie | S7-15 |
| G. T. Macleon | H5-44 |
| R. J. Parazin | H5-49 |
| J. C. Person | T6-09 |
| D. A. Reynolds | R2-11 |
| C. A. Rieck | R3-27 |
| G. J. Rust | T4-01 |
| J. P. Sederburg | R2-11 |
| M. J. Sutey | T4-07 |
| J. E. VanBeek | R3-27 |
| R. J. Van Vleet | H4-62 |
| R. D. Wojtasek | S7-84 |

72 Pacific Northwest Laboratory

| | |
|---|---|
| Z. I. Antoniak | K7-15 |
| J. M. Bates | K7-15 |
| G. H. Beeman | S7-31 |
| S. Q. Bennett | K7-90 |
| P. R. Bredt | P7-25 |
| J. W. Brothers (5) | K5-22 |
| S. A. Bryan | P7-25 |
| J. L. Buelt | P7-41 |
| D. M. Camaioni | K2-44 |
| J. A. Campbell | P8-08 |
| J. B. Colson | K5-10 |
| R. Y. Ecker | K6-91 |
| A. R. Felmy | K9-77 |
| J. A. Fort | K7-15 |
| M. D. Freshley | P8-34 |
| P. A. Gauglitz | P7-41 |
| L. K. Holton | K9-73 |
| J. D. Hudson | K7-15 |
| W. L. Kuhn | K2-21 |
| J. P. Lafemina | K2-25 |
| M. A. Lilga | P8-38 |
| T. E. Michener | K7-15 |
| Y. Onishi (40) | K9-33 |
| F. E. Panisko | P8-34 |
| L. R. Pederson | K2-44 |
| M. R. Powell | P7-14 |
| R. K. Quinn | K9-69 |
| S. D. Rassat | P7-35 |
| H. C. Reid (5) | K7-15 |
| J. R. Rustad | K9-77 |
| W. D. Samuels | K2-44 |
| A. Shekarriz | K7-15 |
| C. W. Stewart | K7-15 |
| J. M. Tingey | P7-25 |
| D. S. Trent (5) | K7-15 |
| P. D. Whitney | K5-12 |
| Information Release (5) | |